AIRFLOW ESTIMATION FROM RESPIRATORY SOUNDS

by

İlhan Yıldırım

B.S., Electrical & Electronics Engineering, Boğaziçi University, 2013

Submitted to the Institute for Graduate Studies in
Science and Engineering in partial fulfillment of
the requirements for the degree of
Master of Science

Graduate Program in Electrical & Electronics Engineering
Boğaziçi University

2018

ACKNOWLEDGEMENTS

Firstly, I would like to express my gratitude to my supervisor, Prof. Yasemin Kahya, for giving me this interesting topic, her guidance and endless patience. I am also deeply grateful to my co-supervisor, Dr. İpek Şen, for her suggestions and practical approach to any kind of problems arised during this study. It was impossible to finish this study without her motivating approach. I also want to thank thesis committee members, Prof. Murat Saraçlar and Assoc. Prof. R. Koray Çiftçi for their comments for future directions.

I would like to thank various members of BUSIM and BETA: Alican Gök, Mehmet Yamaç, Engin Afacan, Emre İşeri, Berk Çamlı, Gürkan Sönmez for their friendship and support. I thank my colleagues Tayyar Güzel, Yeşim Oral and Onur Ertürk for joyful talks about signal processing and engineering.

I am very thankful to my friends: Ozan Şen, Burak Önal, Onur Şen, Merih Çağrı Sağlam, Seçkin Akar, Zafer Zeren, Merve Dökmeci and Dicle Kızılkan for all the moments we have spent together.

Last but not least, my deepest gratitude goes to my parents, Belgin and Ayhan Yıldırım for their endless love and support. I thank my brother, Sinan Yıldırım, for his encouragement and support.

ABSTRACT

AIRFLOW ESTIMATION FROM RESPIRATORY SOUNDS

The aim of this study is estimate the respiratory airflow and phases from the respiratory sounds recorded at the chest wall. In order to estimate the absolute airflow curve, time varying autoregressive (TVAR) model coefficients are used. TVAR coefficients are calculated with three approaches: windowing based autoregressive modeling, TVAR modeling with basis functions, TVAR modeling with Kalman filter. Then evolution in magnitudes of spectral band is used as an estimation of airflow curve. A Wiener filter approach is presented for fusion of different features to estimate the airflow curve. Average of correlation coefficients up to 0.75 for absolute airflow and 0.72 for airflow are achieved. In the second part of this thesis, respiratory phases are estimated using a neural network and the estimated absolute airflow curve. TVAR coefficients, Shannon entropy estimate, percentile frequencies, variance, spectral magnitude and kurtosis are used as inputs. Distributions of these features for different phases and Kullback Leibler divergence of these distributions are presented. For phase estimation from estimated airflow, heuristic methods are used for local minima extraction and selection of the transition points. 97 and 83 milliseconds (3% and 2.6% of average full cycle) of average deviation from true transition point are achieved with neural networks for inspiration to expiration and expiration to inspiration transitions respectively. 120 and 131 milliseconds (3.8% and 4.1% of average full cycle) of average deviation from true transition point are achieved with heuristic methods for inspiration to expiration and expiration to inspiration transitions, respectively.

ÖZET

SOLUNUM SESLERİNDEN SOLUK AKIŞI KESTİRİMİ

Bu çalışmanın amacı soluk akış hızını ve yönünü sırttan alınan solunum seslerini kullanarak tahmin etmektir. Soluk akış hızının mutlak değerini tahmin etmek için zamanla değişen özbağlanımlı (ZDÖB) model katsayıları kullanılmıştır. ZDÖB model katsayıları üç farklı yöntem ile hesaplanmıştır: kayan pencereler, doğuray vektörler ile modelleme, Kalman süzgeci ile modelleme. Sıklık bantlarındaki genliğin zamanda değişimi de soluk akış hızının kestirimi olarak kullanılmıştır. Wiener süzgeci yaklaşımı farklı kestirimlerin kaynaşımı için kullanılmıştır. Mutlak akış hızı için 0.75, akış hızı için 0.72 ilinti katsayılarına ulaşılmıştır. Bu çalışmanın ikinci kısmında soluk evreleri yapay sinir ağları ve akış hızı kestirimi kullanılarak kestirilmiştir. ZDÖB model katsayıları, Shannon entropi kestirimi, yüzdelik frekanslar, değişinti, spektral genlik ve kurtosis yapay sinir ağının girdisi olarak kullanılmıştır. Bu özelliklerin farklı evreler için dağılımları arasındaki Kullback-Leibler ıraksaklıkları sunulmuştur. Akış hızı kestiriminden evre kestirilmesi için yerel en küçükleri ve geçiş noktaları bulmak için buluşsal yöntemler sunulmuştur. Yapay sinir ağları ile kestirimde geçiş noktalarından sapma soluk verme evresinden alma evresine ve alma evresinden verme evresine geçişte sırasıyla 97 ve 83 milisaniye (tam bir soluk alış veriş döngüsünün %3 ve %2.6'sı) olarak hesaplanmıştır. Bu değerler, buluşsal yöntemler ile akış hızı kestirimi kullanılması durumunda 120 (%3.8) ve 131 (%4.1) milisaniye olarak hesaplanmıştır.

TABLE OF CONTENTS

LIST OF FIGURES

LIST OF TABLES

LIST OF SYMBOLS

a_i	i^{th} autoregressive coefficient
$c_{i,j}$	Scale factor of j^{th} basis function on i^{th} autoregressive coefficient
$E[X]$	Expected value of X
e	White Gaussian noise
F	State transition matrix
H	State ob
R_{XX}	Autocovariance matrix of random process X
$r_{XX}(i)$	i^{th} autocorrelation coefficient of random process X
u	Basis function
μ_X	Mean of random variable X
σ_X	Standard deviation of random variable X

LIST OF ACRONYMS/ABBREVIATIONS

ACF	Autocorrelation Function
AR	Autoregressive
FFT	Fast Fourier Transform
KL	Kullback Leibler
LV	Log of Variance
STFT	Short Time Fourier Transform
TVAR	Time Varying Autoregressive

1. INTRODUCTION

Auscultation of respiratory sounds with an aim to gain information about respiratory diseases is a diagnosis method which has been applied for at least 2400 years. Since then, different auscultation techniques have been used. The most widely used tool developed for this purpose is called "stethoscope" and it is invented in 1816 by Rene Laënnec [2]. Medical doctors still use this device to diagnose several diseases such as asthma, bronchitis etc.

In recent decades, engineers started to work on respiratory sounds and they produced electronic stethoscopes. These electronic stethoscopes have some advantages over the traditional ones. First of all, the frequency band is not limited [3] by the mechanic structure of stethoscope and the sounds can be recorded for subsequent referral. Another advantage is that the respiratory sound recordings have made analyzing the sound with the help of computers possible.

In recent years, together with developing classification techniques, there has been a great effort in automatic classification of respiratory sounds as healthy or pathological [1, 4]. Some of these methods are dependent not only on sounds but also on the airflow information [5]. Airflow is usually recorded by an instrument, called pneumotachograph. This instrument is difficult to use with subjects with disabilities or very small children.

Main motivation of this thesis is to estimate the airflow and respiratory phases from the respiratory sounds recorded at the chest wall without using pneumotachograph so as to enable easier airflow measurements to be and to contribute to the development of a single handheld electronic stethoscope whose sound recording will be enough for automatic diagnosis.

Before the preview of the work of this thesis, brief review of the literature on the relation between flow, phase and respiratory sounds is presented.

Lessard and Wong [6] reported that the relation between the spectral parameters which are mean frequency, frequency of maximum power and the highest frequency at which the power in the spectrum is at least 10 percent of maximum power, and flow rate is not linear and spectral parameters saturate as the flow rate goes beyond 0.75 l/s.

Yadollahi and Moussavi [7] suggested using entropy of bandpass filtered tracheal sounds of overlapping windows whose durations are 100 milliseconds. They achieved average error of 7.3 % and 7.4 % for inspiratory and expiratory phases after calibrating the model which uses the entropy information.

Huq and Moussavi [8] proposed using log of variance (LV) to detect onsets from tracheal sounds. For phase identification, they used 4 parameters calculated over the LV curve and the duration of the phase. They developed and tested the method for tracheal sounds and it is reported that 95.6% accuracy was achieved for phase identification after onsets are verified by visual inspection.

Moussavi et al. [9] suggested using tracheal sounds for onset detection and the power difference in 150-450 Hz at the "best recording position", where the difference in power for inspiration and expiration is greatest, for phase identification. It is reported that the success rate in phase identification is 100% after the onsets are found.

Golabbakhsh et al. [10] suggested using the average power calculated over the frequency band between 150-450 Hz (P_{ave}) of tracheal sounds to estimate the respiratory flow. They have two approaches, first one is expressing the flow ($\hat{F}$) as a linear function of log of P_{ave} as in 1.1 and the other one is training an adaptive filter with

three taps (w_1, w_2 and w_3), whose input is P_{ave} as in 1.2.

$$\hat{F} = c_0 + c_1 \log(P_{ave}) \tag{1.1}$$

$$\hat{F} = \sum_{i=1}^{M} w_i P_{ave} \tag{1.2}$$

Çiftçi and Kahya [11] modeled the sounds recorded at both trachea and chest wall as time varying autoregressive (TVAR) processes by using Fourier basis functions and used the first autoregressive (AR) coefficient vector as the estimate of absolute airflow curve. Reported correlations for sounds recorded at trachea and chest wall were 0.9 and about 0.6 (extracted from figure in paper) respectively.

Organization of thesis is as follows:

In chapter 2, the experimental setup and data is explained.

In chapter 3, AR and TVAR processes and the methods to find TVAR coefficients of a signal are described where windowing based AR modeling and TVAR modeling with basis functions and Kalman filter are used. Short Time Fourier Transform (STFT) and Wiener filter which is used to unify different estimations are also presented. Finally experiments and results are presented.

In chapter 4, the method for period estimation is given first. Then neural networks approach and features is explained. After neural networks, the method which estimates the transition points and then identifies the phases between estimated transition points will be described. Lastly, experiments and results are documented.

In the last chapter, conclusion on this work are drawn.

Main contributions of this thesis are as follows:

- The relation between autoregressive model coefficients or respiratory sounds recorded at the posterior chest and the airflow curve is analyzed.
- The relation between power in different frequency bands and airflow curve is analyzed.
- Different estimations of airflow curve are combined using a Wiener filter approach.
- Distribution of different features for inspiration and expiration phases are analyzed.
- A robust period estimation method based on autocorrelation function is presented.
- A neural network is used with different features to estimate respiratory phase from recorded sounds.
- To the best of our knowledge, a naive method to select transition points from a set of candidate points is presented.

2. EXPERIMENTAL SETUP AND DATA

The data used throughout this thesis is taken from the database belonging to Boğaziçi University Lung Acoustics Laboratory. All sound and airflow samples were recorded with the device developed in this laboratory [12]. The recording device has 14 channels. Each channel has the same analog interface, which includes a Sony ECM-44 BPT electret microphone followed by an analog amplifier with gain of 100 which has a instrumentation amplifier based design. The amplification unit is followed by a 6^{th} order Butterworth low pass filter which has 4000 Hz cut-off and a 8^{th} order Bessel high pass filter whose cutoff is 80 Hz. The airflow recordings were done with a Validyne CD379 pneumatachograph. The digitization unit is the National Instrument's DAQCard-6024E which operates at 9600 Hz and has 12 bit resolution. Each recording has a duration of 15 seconds [12].

The subject set of this study consists of 23 healthy adult subjects. The sounds were recorded at 14 different locations on the chest wall. Locations of channels are shown in 2.1. In this study, respiratory sounds recorded from the channels between 1 and 12 are used.

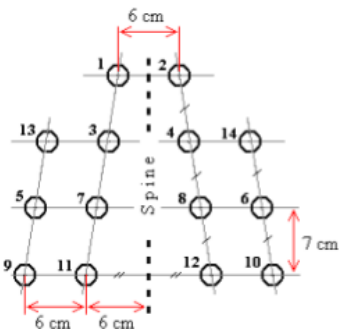

Figure 2.1. Microphone Locations on the Chest Wall [1]

3. AIRFLOW CURVE ESTIMATION

3.1. Autoregressive Models

Autoregressive modeling is a widely used method in spectral signal analysis. It is also used in respiratory signal analysis and since the respiratory sounds have spectral characteristics changing over time, either the sound is divided into small frames and it is assumed that the small frames are stationary or the respiratory sounds are modeled as time varying autoregressive processes. It is reported that when a respiratory sound signal is modeled as TVAR process, the first AR coefficient is highly correlated with the airflow for the sounds recorded at trachea and have smaller correlation for the sounds recorded at the chest wall [11]. The sounds recorded at the chest wall are tested to find best settings for highest correlation in this subsection. The AR coefficients are extracted using three methods:

- Windowing Based Autoregressive Modeling: Divide the signal into overlapping windows with the assumption that each window is independent of others.
- Time Varying Autoregressive Modeling with Basis Functions: Assume the AR parameters are combination of sinusoidal signals.
- Time Varying Autoregressive Modeling with Kalman Filter: Assume the AR parameters are changing slowly.

3.1.1. Univariate Autoregressive Model

Univariate AR model is a difference equation where the current measurement of the signal is a linear combination of past measured values and a white Gaussian noise. The model is equivalent to a filter with infinite impulse response where the input is white Gaussian noise. The equation of an AR model is given in (3.1). In this equation a_i is the i^{th} order AR coefficient, N is the order of model and e is the noise term where

$\mu_e = 0$ and σ_e^2 is constant [13].

$$x(n) = \sum_{i=1}^{N} a_i x(n-i) + e(n) \tag{3.1}$$

Before looking at mean, variance, autocorrelation and spectral content of a general AR model, we must set some conditions on a_i's to make the model stationary. The stationarity requires that the mean, variance and autocorrelation function are constant. If the mean is constant then (3.2) must hold. We know that μ_e is 0, then either $\sum_{i=1}^{N} a_i = 1$ or $\mu_x = 0$ is true.

$$\mu_x = \sum_{i=1}^{N} a_i \mu_x + \mu_e \tag{3.2}$$

We require $E[X(0)] = 0$ for initial conditions for AR processes and it ensures $\mu_x = 0$. Then for variance we can write the equations in (3.3), (3.4) and (3.5).

$$\sigma_X^2 = E[X(n)X(n)] - \mu_X^2 \tag{3.3}$$

$$\sigma_X^2 = \sum_{i=1}^{N} a_i E[X_n X_{n-i}] + E[X_n e_n] - \mu_X^2 \tag{3.4}$$

$$\sigma_X^2 = \sum_{i=1}^{N} a_i R_{XX}(i) + \sigma_e^2 \tag{3.5}$$

We know that autocorrelation coefficients are very important in the analysis of an AR model. The AR coefficients can be directly calculated in the presence of the

autocorrelation coefficients.

$$r_{xx}(i) = R_{xx}(i)/R_{xx}(0) \tag{3.6}$$

$$r_{xx}(i) = E[x(n)x(n-i)]/R_{xx}(0) \tag{3.7}$$

$$r_{xx}(i) = \frac{\sum_{j=1}^{N} E[a_j x(n-j)x(n-i)]}{R_{xx}(0)} \tag{3.8}$$

$$r_{xx}(i) = \sum_{j=1}^{N} a_j r_{xx}(i-j) \tag{3.9}$$

The equation in (3.9) is very useful since we can rewrite it as in (3.10), this equation is called Yule-Walker equation. So, given a signal generated with an AR model, we can find the coefficients of that model by solving the equation in (3.10). Let's call this equation as $r = Ra$, the the coefficients can easily be found with $a = R^{-1}r$.

$$\begin{pmatrix} r_{XX}(1) \\ r_{XX}(2) \\ \vdots \\ r_{XX}(N-1) \\ r_{XX}(N) \end{pmatrix} = \begin{pmatrix} 1 & r_{XX}(1) & ... & r_{XX}(N-2) & r_{XX}(N-1) \\ r_{XX}(1) & 1 & ... & ... & r_{XX}(N-2) \\ \vdots & \vdots & \vdots & \vdots & \vdots \\ r_{XX}(N-2) & ... & ... & 1 & r_{XX}(1) \\ r_{XX}(N-1) & r_{XX}(N-2) & ... & r_{XX}(1) & 1 \end{pmatrix} \begin{pmatrix} a_1 \\ a_2 \\ \vdots \\ a_{N-1} \\ a_N \end{pmatrix} \tag{3.10}$$

Although solving the equation (3.10) seems to be very straightforward, it requires exact knowledge on correlation coefficients. However, when we are given a signal with finite length we can just estimate the correlation coefficients, and the error in calculated AR coefficients will depend on the condition number of R matrix. To solve this equation, there are several methods in literature, throughout this thesis we will use Burg's Method to find the AR coefficients, since it is more stable than the others [14].

```
1: procedure WindowedAR(signal, order, winLen, overlap)
2:     windowStart ← 1; L ← Length(signal);
3:     while windowStart ≤ L − winLen do
4:         temp ← signal(windowStart : (windowStart + windowLength));
5:         AR(:, i) ← EstimateAR(temp, N);
6:         windowStart ← windowStart + windowLength;
7:     end while
8:     return AR;
9: end procedure
```

Figure 3.1. AR Coefficients Estimation With Overlapping Windows

3.1.2. Time Varying Autoregressive Model

While univariate autoregressive model is very useful for many signals, the method does not use the continuity of the signal and treats each segment independently. Assuming that the coefficients at different time instants are correlated with each other and building some structured models is another method which is widely applied for nonstationary signals. TVAR modeling was applied to respiratory signals and satisfactory results have been obtained in many papers. The equation describing a TVAR process is given in (3.11).

$$x(n) = \sum_{i=1}^{N} a_i(n)x(n-i) + e(n) \tag{3.11}$$

We will use two methods for solving this equation for a_i's. One of them is modeling a_i's as combination of sinusoids, the other one is modeling a_i's as slowly changing parameters.

3.1.2.1. TVAR Coefficients Estimation With Fourier Basis Functions. In this method, the AR coefficients are assumed to be combination of sinusoidal functions,as given in

equations in (3.12) and (3.13).

$$x(n) = \sum_{i=1}^{N} x(n-i) \sum_{j=1}^{M} c_{ij} u_j(n-i) + e(n) \tag{3.12}$$

$$a_i(n) = \sum_{j=1}^{M} c_{ij} u_j(n-i) \tag{3.13}$$

Equation (3.12) can be rewritten in vector form as in (3.14) where X_i is the diagonal matrix where the diagonal elements are adjacent elements of x starting from i, U is the matrix whose columns are basis vectors, and the c_i's are the unknown parameters in this equation.

$$x = \sum_{i=1}^{N} X_i U c_i + e \tag{3.14}$$

Let $Y_i = X_i U$, the equation can be written in matrix form as in

$$x = \left(Y_1 | Y_2 \dots Y_N \right) \begin{pmatrix} c_1 \\ c_2 \\ \vdots \\ c_M \end{pmatrix} + e \tag{3.15}$$

The equation in (3.15) describes an overdetermined set of equations, and least squares approach is used to solve this. After finding $\mathbf{c}$ vector, which has NxM elements, calculating $a_i(n)$, TVAR coefficients, is straightforward.

$$\mathbf{c} = (Y^T Y)^{-1} Y^T x \tag{3.16}$$

Experiments are carried out to find the optimum values for the AR order, the number of basis vectors, and the range of frequencies spanned by basis vectors to get the best correlation.

```
1: procedure TVARFourierBasis(signal, order, freqRange, numBasis)
2:     δ_f = freqRange/numBasis;
3:     for i=1:numBasis do
4:         U(:, 2*i − 1) = sin(i*δ_f);
5:         U(:, 2*i) = cos(i*δ_f);
6:     end for
7:     Generate Y: Project signal onto U;
8:     c = (Y^T Y)^{-1} Y^T x
9:     for i=1:N do
10:        AR(:, i) = U c_i;
11:    end for
12:    return AR;
13: end procedure
```

Figure 3.2. TVAR Coefficients Estimation With Fourier Basis Functions

3.1.2.2. TVAR Coefficients Estimation With Kalman Filter. Kalman filter is a very old but still popular algorithm in the field of information processing. It is the minimum mean square estimator for the state of linear dynamical systems [15]. It is used in a wide range of areas from tracking applications to computer games.

Before explaining how Kalman filter works, the required equations to describe the model where it is applied are given. Kalman filter is invented to work on dynamic systems where we can record the noisy observations of transformations of the process in interest. So two equations may be given, for both measurement (3.17) and process

(3.18) model [16].

$$y_n = H_n x_n + v_n \tag{3.17}$$

$$x_n = F_n x_{n-1} + B_n u_n + w_n \tag{3.18}$$

In (3.17) the H is the transform matrix and v is the measurement noise. In (3.18) x is the state vector, u is control input to the system, B is the control matrix, F is the state transition matrix and w is process noise. When a model desribed in (3.17) and (3.18) and measurements of y are present, Kalman filter can be used to estimate x. When the process and measurement noises are Gaussian then Kalman is the optimal estimator.

In our problem, there is not any control input to system and equations convert to (3.19) and (3.20). In these equations y is the recorded sound amplitude, x is the AR coefficients, H is equal to raw vector containing previous N values of y where N is the AR order.

$$y_n = H_n x_n + v_n \tag{3.19}$$

$$x_n = F_n x_{n-1} + w_n \tag{3.20}$$

Kalman filter includes two stages, prediction and measurement update. The prediction equations are given in (3.21) and (3.22). The measurement update equations are given in (3.23), (3.24) and (3.25). In these equations $\hat{x}_{n|m} = E[x_n|y_{1:m}]$ and $P_{n|m} = E[(x_n - \hat{x}_{n|m})(x_n - \hat{x}_{n|m})^T|y_{1:m}]$.

Prediction:

$$\hat{x}_{n|n-1} = F\hat{x}_{n-1|n-1} \tag{3.21}$$

$$P_{n|n-1} = FP_{n-1|n-1}F^T + \sigma_w^2 \tag{3.22}$$

Measurement Update:

$$K_n = P_{n|n-1}H(H_n^T P_{n|n-1}H_n + \sigma_v^2)^{-1} \tag{3.23}$$

$$\hat{x}_{n|n} = \hat{x}_{n|n-1} + K_n(y_n - H_n^T\hat{x}_{n|n-1}) \tag{3.24}$$

$$P_{n|n} = (I - K_n H_n^T)P_{n|n-1} \tag{3.25}$$

In the equations above, the filter uses only past values to estimate current value of x. In order to add the information from complete signal, the estimations can be smoothed with Rauch-Tung-Striebel backward recursions given in (3.26), (3.27) and (3.28).

$$J_n = P_{n|n}F^T P_{n+1|n}^{-1} \tag{3.26}$$

$$\hat{x}_{n|N} = \hat{x}_{n|n} + J_n(x_{n+1|N} - x_{n+1|n}) \tag{3.27}$$

$$P_{n|N} = P_{n|n} + J_n(P_{n+1|N} - P_{n+1|n})J_n^T \tag{3.28}$$

In these equations process noise, state transition matrix and measurement noise are not being updated, and they need to be tuned. The tuning process and results are given in the Experiments & Results section.

3.2. Time Frequency Analysis

Short Time Fourier Trasnform is a technique which is widely used and very useful for the analysis of signals with a time varying spectral characteristics. STFT is used for the analysis of respiratory signals since they have a nonstationary nature.

$$X_m(f) = \sum_{n=-\infty}^{\infty} x(n)w(n - mR)e^{-j2\pi fn} \tag{3.29}$$

STFT is defined in (3.29). It can be seen as a sliding Fourier Transform (FT) [17]. In this equation, R is hop size and w is the window function which is zero outside of a predefined range and is used to pick the part of signal which is the input of FT and to smooth the signal to make it stationary. The window is an important parameter for STFT, it is the effective parameter to adjust time-frequency resolution. First of all, the window length must be so small that it must ensure that the selected portion is stationary. There is also a trade-off between resolution in time and resolution in frequency, this trade-off is also controlled with window length. As the window length increases the frequency resolution increases and the time resolution decreases. So, for wideband signals one can use smaller window lengths whereas for narrowband signals greater window lengths may be used.

The output of STFT operation is a two dimensional complex matrix, which describes the magnitude and phase of frequency band component. For most of the applications, including respiratory sounds, the magnitude information is needed and the complex matrix is converted to a real matrix which gives information about energy directly. The resulting matrix is usually visualized by a heatmap as in 3.3.

In Figure 3.3, a sample of respiratory sound, magnitude plot of its STFT and corresponding airflow are depicted and it is observed that a relationship exists between the airflow and some horizontal lines. These horizontal lines correspond to the energy

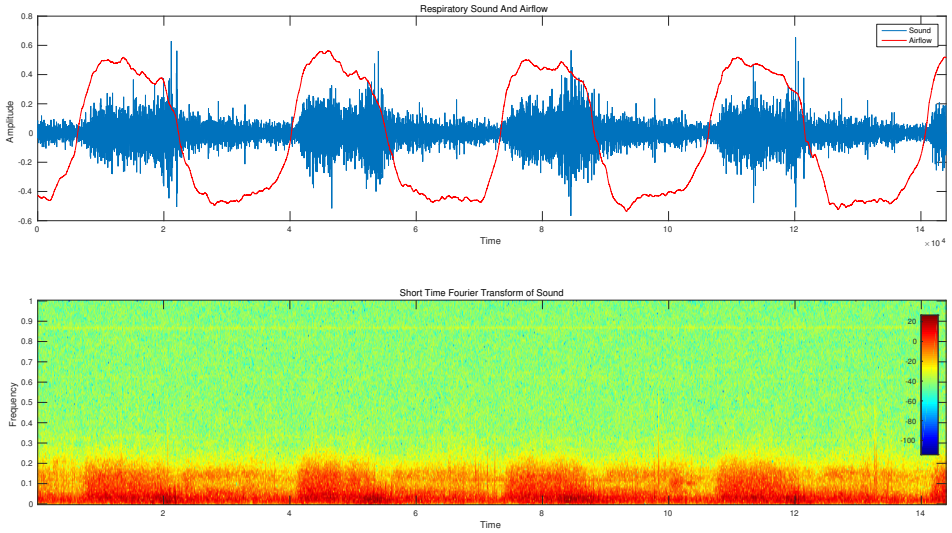

Figure 3.3. A respiratory sound, corresponding airflow and STFT magnitude plot

at a frequency band over the time. Experiments are run to test the correlation between the evolution of energy at each frequency band with the airflow. The STFT is tuned by tweaking the window type, window length and number of FFT bins as given in the Experiment & Results section.

3.3. Unifying Estimations

When we have an estimation problem with desired output, d and observations in x vector, if each observation in x and d are jointly wide sense stationary (wss), the optimum estimator for mean square error (MSE) is the Wiener filter [18]. We can write down the equations and derive the optimum filter. The estimation equation is given in (3.30) where $\hat{d}$ is the estimation in this equation. Estimation error is given in (3.31)

and the error measure we are interested in is given in (3.33)

$$\hat{d} = \sum_{i=1}^{N} w_i x_i = \mathbf{w^T x} \tag{3.30}$$

$$e = d - \hat{d} = d - \mathbf{w^T x} \tag{3.31}$$

$$E[e^2] = E[|d - \hat{d}|^2] \tag{3.32}$$

$$E[e^2] = E[d^2 - 2d\mathbf{x^T w} + \mathbf{w^T x x^T w}] \tag{3.33}$$

In order to minimize the error we can differentiate with respect to $\mathbf{w}$ and find the value where the derivative is zero. For error to be at its minimum the expectation in (3.34) must be zero, which requires $\mathbf{x}$ and e to be uncorrelated.

$$\frac{\partial E[e^2]}{\partial \boldsymbol{w}} = 2E[e\frac{\partial e}{\partial \boldsymbol{w}}] = -2E[ex_i] \tag{3.34}$$

If we rewrite error as the difference between d_n and $\mathbf{w_{opt}^T x}$, then we can state the equations in (3.35) and (3.36).

$$E[(d_n - \mathbf{w_{opt}^T x})\mathbf{x}] = 0 \tag{3.35}$$

$$E[\mathbf{x x^T}]\mathbf{w_{opt}} = E[\mathbf{x}d_n] \tag{3.36}$$

The first expectation in (3.36) is the autocovariance matrix of $\mathbf{x}$ and the second expectation is the crosscovariance between x and d. The filter w_{opt} is called as the Wiener filter.

In previous sections, vectors which are estimations of airflow are obtained. A weighted sum of these estimations are used as observations and weights are decided by using this Wiener filter approach. A block diagram explaining this method is given in

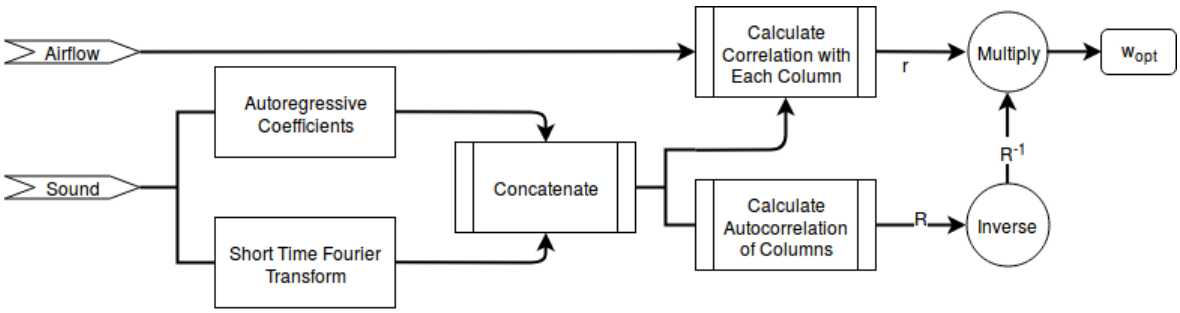

Figure 3.4. Block diagram explaining the Wiener approach to unify the estimations

Figure 3.4.

3.4. Experiments & Results

In this section, the experiments to obtain the best tuning parameters and the results using the methods explained in this chapter are presented.

3.4.1. Univariate Autoregressive Model

There are four parameters to be optimized in the univariate autoregressive modeling method. These parameters are the coefficient degree, AR order, window length and overlap amount.

First the problem of finding the best AR order and coefficient order is addressed. For this purpose, experiments are done for AR orders from 1 to 15 with window length of 500, and 50% overlap.

It can be inferred from Figures 3.5 and 3.6 that the correlation is decreasing with increasing coefficient order and the correlation with absolute value of flow is significantly greater than the correlation with real value of flow. It is decided to continue the analysis with absolute value of airflow for AR estimators. In order to find the best model order experiments are run with window length 500 and an overlap of %50 with model orders from 1 to 15. The results are shown in Figure 3.7. As can be seen from

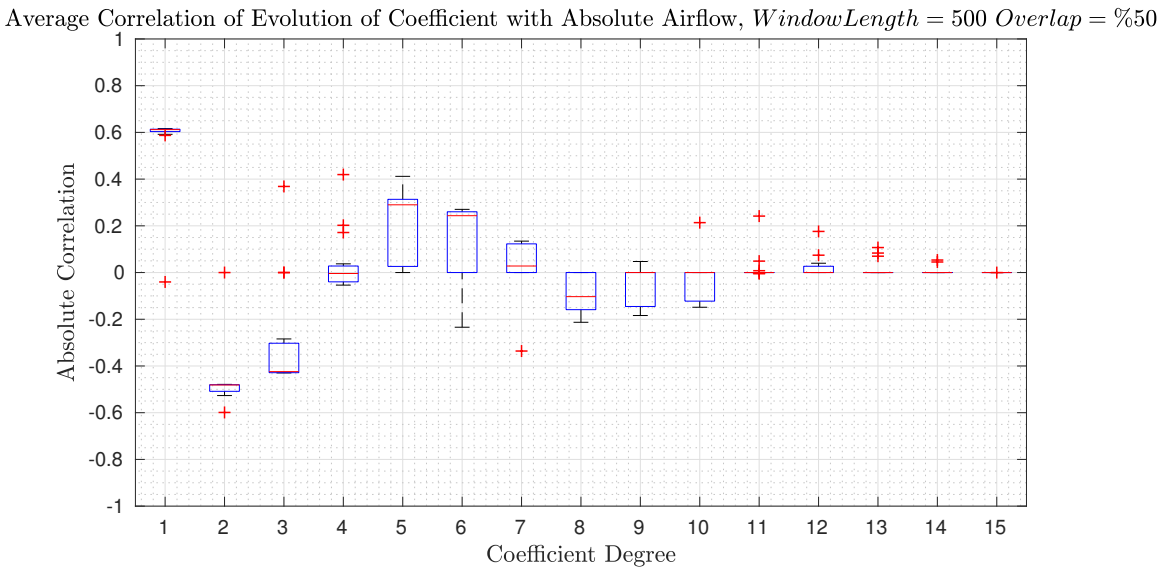

Figure 3.5. Boxplot for correlation coefficient of AR coefficient evolution with absolute value of airflow for different coefficient orders

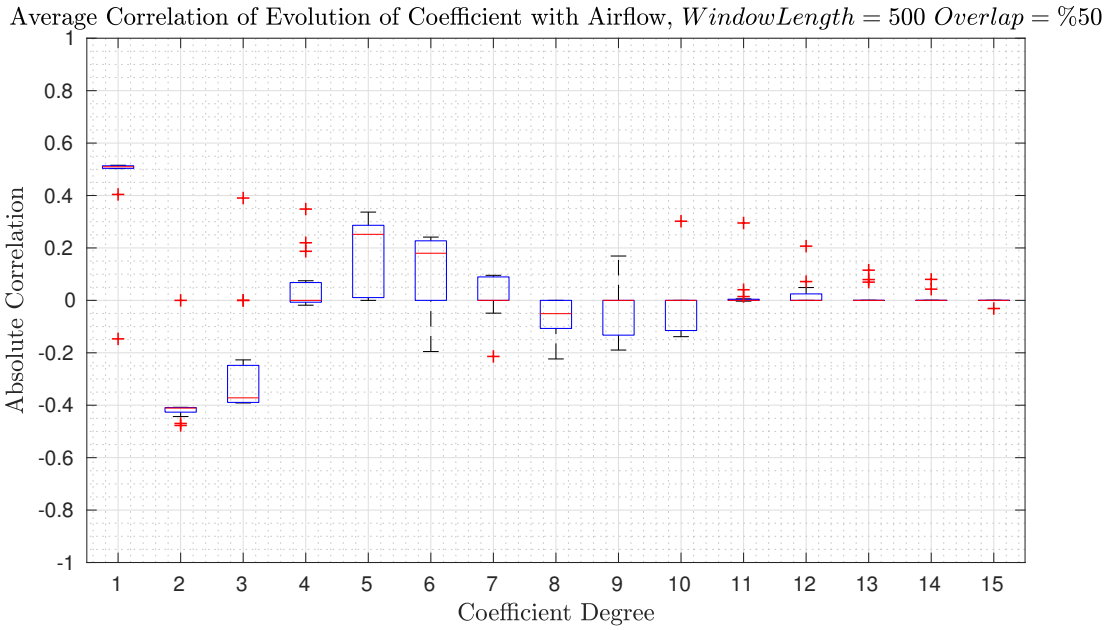

Figure 3.6. Boxplot for correlation coefficient of AR coefficient evolution with airflow for different coefficient orders

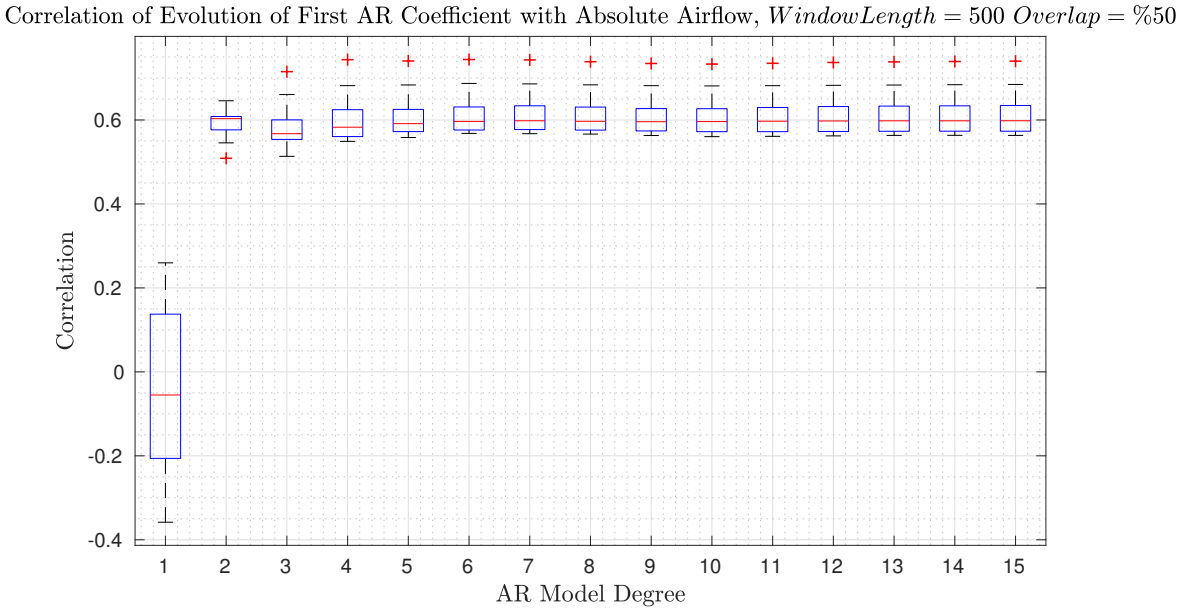

Figure 3.7. Boxplot for correlation coefficient of AR coefficient evolution with airflow for different AR model orders

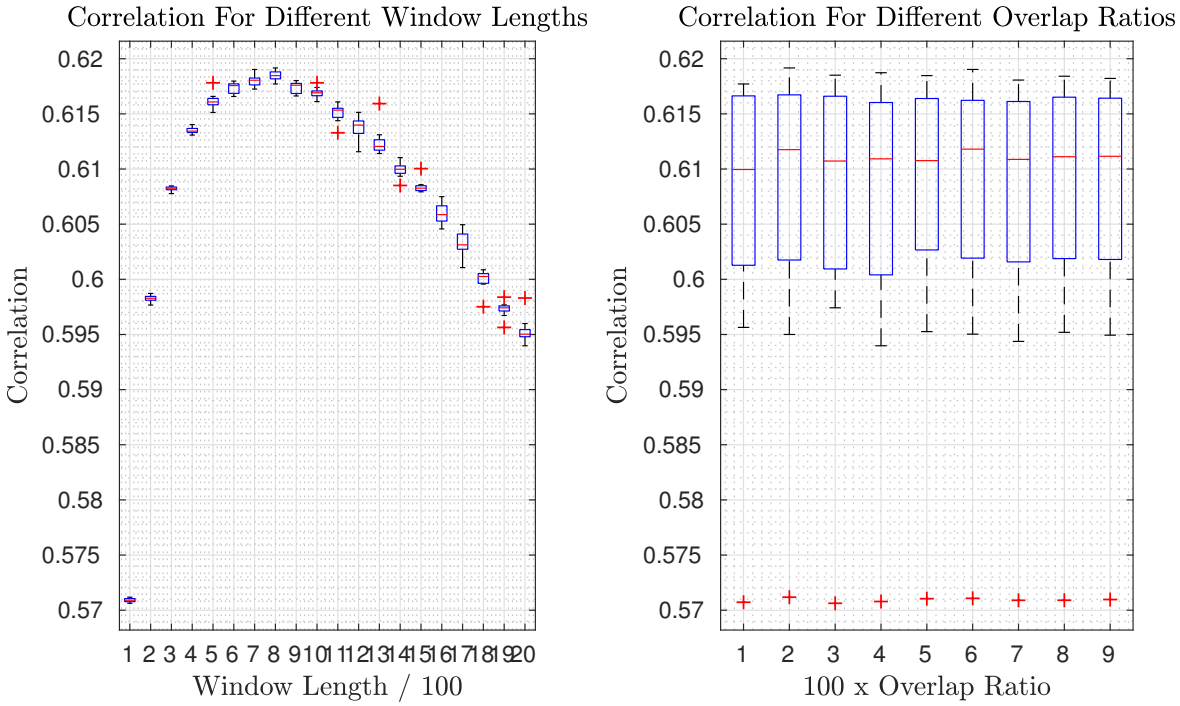

Figure 3.8. Boxplot for correlation coefficient of first AR coefficient evolution with absolute airflow for different window lengths and overlap ratios

the Figure, there is not any significant difference after sixth order AR model, so model order 6 is chosen. After selecting model order, the window length and overlap ratio are left to be decided on. In order to select them experiments are run with window lengths from 100 to 2000 with a step size of 100 and overlap ratios from 10% to 90% with a step size of 10%. The results for different window lengths and overlap ratios are summarized in Figure 3.8. According to the results, best window length is 800 and changing the overlap ratio does not generate any difference in the correlation. In the final experiments, 90% overlap is used to increase the resolution.

The resulting decision for univariate autoregressive solution with overlapping windows is 6, 800 and 90% for model order, window length and overlap ratio, respectively.

3.4.2. Time Varying Autoregressive Model with Basis Functions

The parameters for this method are model order, number of basis functions and the frequency difference in adjacent basis functions.

First, experiments to determine the best model order are run with model orders from 1 to 15 where the number of basis functions are 201 (100 sines, 100 cosines and a constant) and the separation in frequency is 0.04 Hz. Experiment results are given in Figure 3.9. Highest correlation is achieved with the model order of 6 again.

After deciding on the model order, it is needed to decide on the number of basis functions and the frequency separation of basis functions. Before doing this, experiments are run to determine the frequency coverage for highest correlation and run experiments with frequency step size of 0.025 Hz and different number of basis vectors from 50 to 300 with a step size of 50. The results are given in Figure 3.10. According to test results, 5 Hz is enough to cover for best results.

Finally simulations are run to decide both the number of basis frequencies and

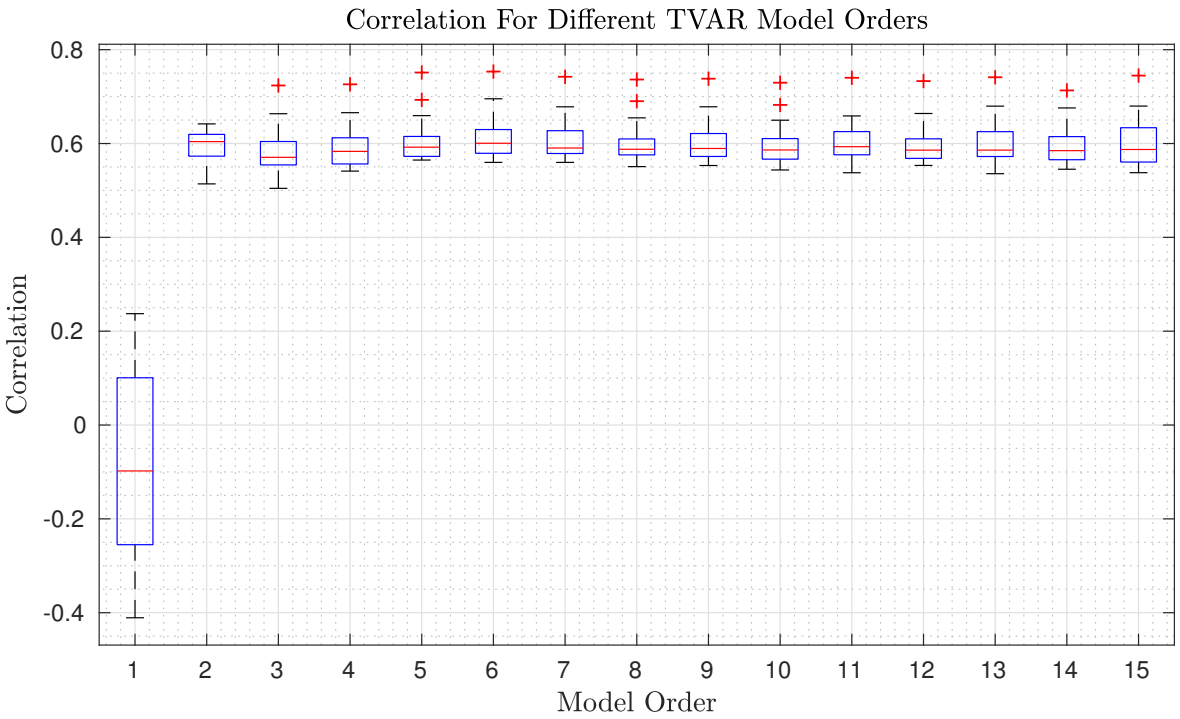

Figure 3.9. Boxplot for correlation coefficient of first AR coefficient evolution with absolute airflow for different TVAR model orders

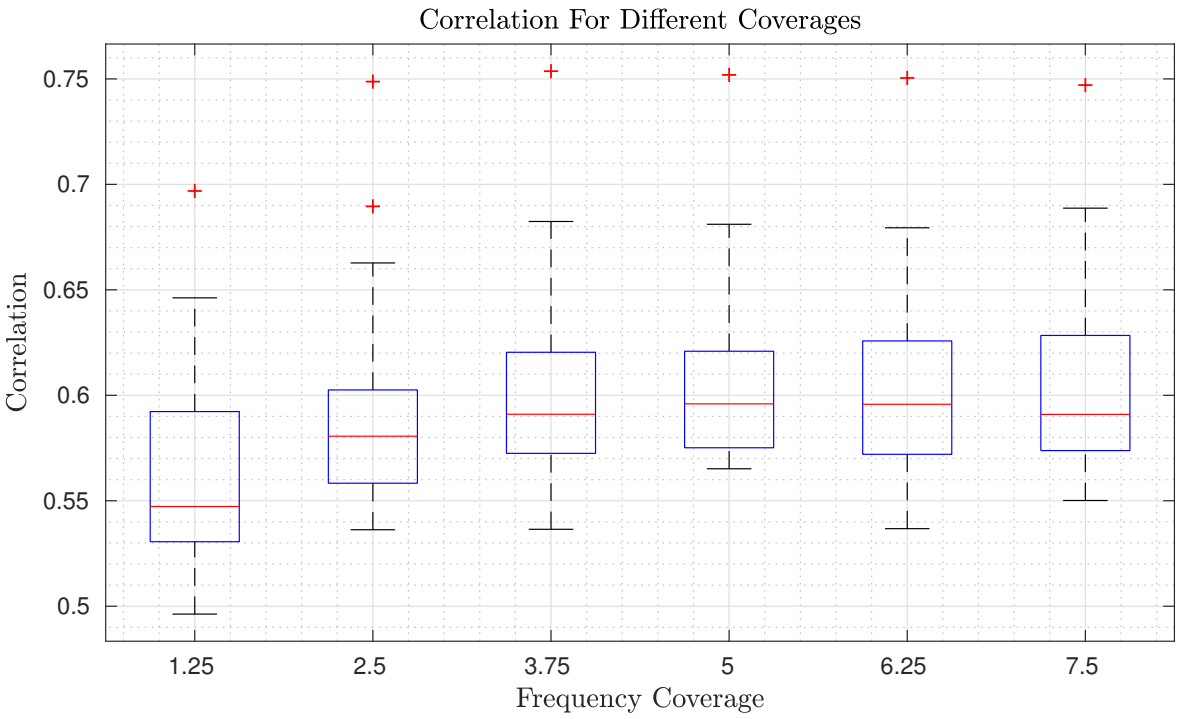

Figure 3.10. Boxplot for correlation coefficient of first AR coefficient evolution with absolute airflow for different frequency coverage

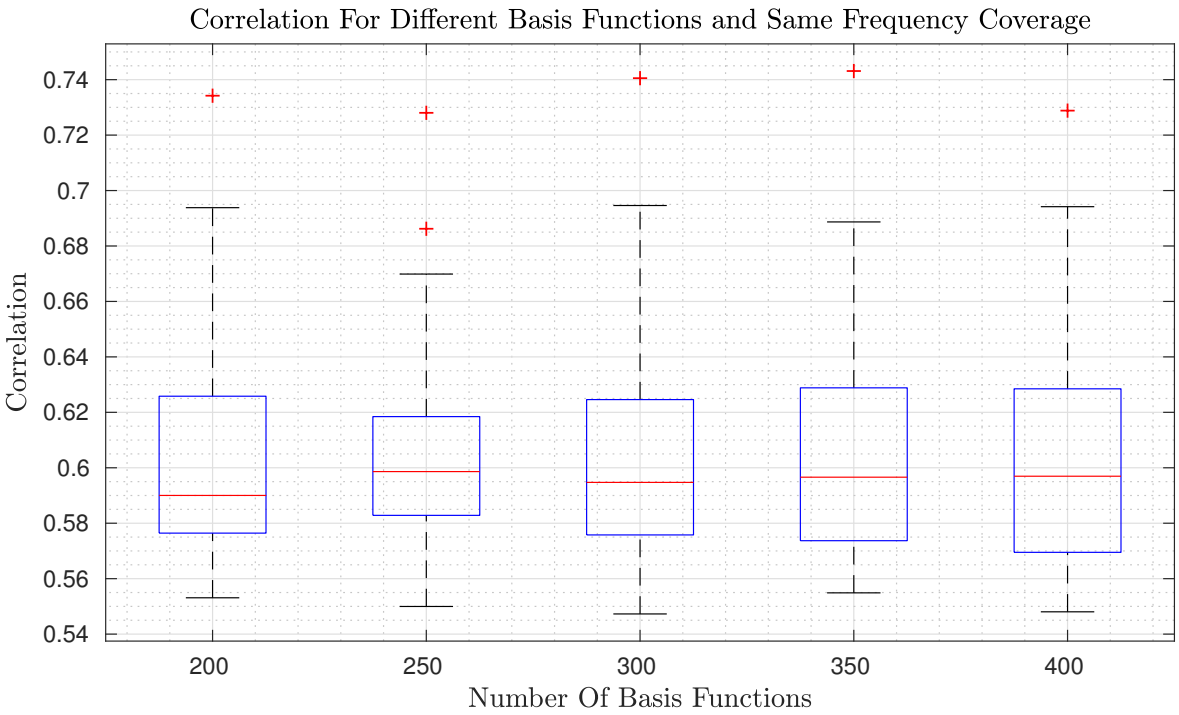

Figure 3.11. Boxplot for correlation coefficient of first AR coefficient evolution with absolute airflow for number of basis functions

frequency separation where the frequency range from 0 to 5 Hz is covered. The results are given in Figure 3.11. It can be seen that there is no significant change for the number of basis functions from 200 to 400. 250 is chosen for minimum standard deviation.

To summarize, 6, 250, 0.02 are chosen for model order, number of basis frequencies and frequency separation, respectively.

3.4.3. Time Varying Autoregressive Model with Kalman Filter

For this method, the estimated noise variance by windowing based AR modeling as the measurement noise variance. The best noise variance for process noise is found by experiments. Simulations where the process noise variance goes from 0.0002 to 0.004 with a step size of 0.0002 are run. The results are given in Figure 3.12. 0.004 is chosen as the process variance.

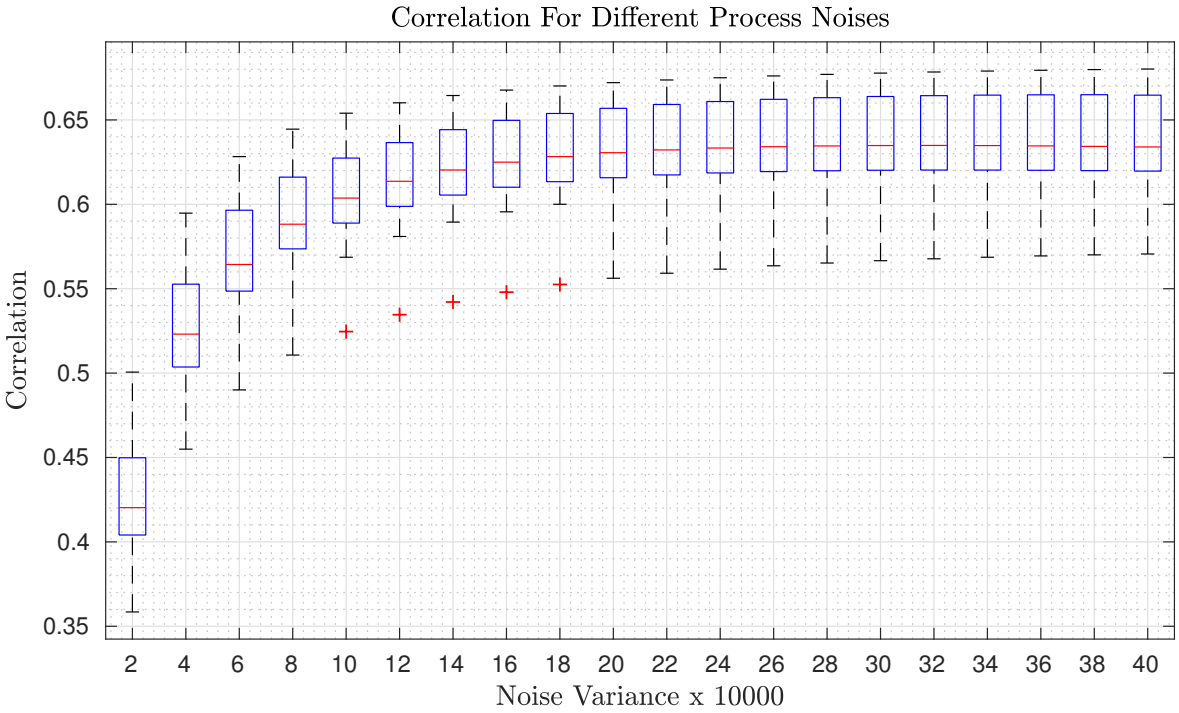

Figure 3.12. Boxplot for correlation coefficient of first AR coefficient evolution with absolute airflow for different process noise variances

3.4.4. Short Time Fourier Transform

Experiments were run with 64, 128 and 256 FFT bins and window lengths of 128, 256, 512, 1024 and 2048. The results are shown in Figures 3.13, 3.14 and 3.15. The conclusion is the greatest correlation is achieved between 150 and 450 Hz.

3.4.5. Unifying Estimations

Simulations were run with different number of vectors to be unified, where the vectors are outputs of univariate AR and STFT methods.

3.4.6. Results

The resulting correlation coefficients are given in Figure 3.17. Average correlation coefficients with absolute airflow curve are 0.63, 0.63 and 0.65 for windowing based AR

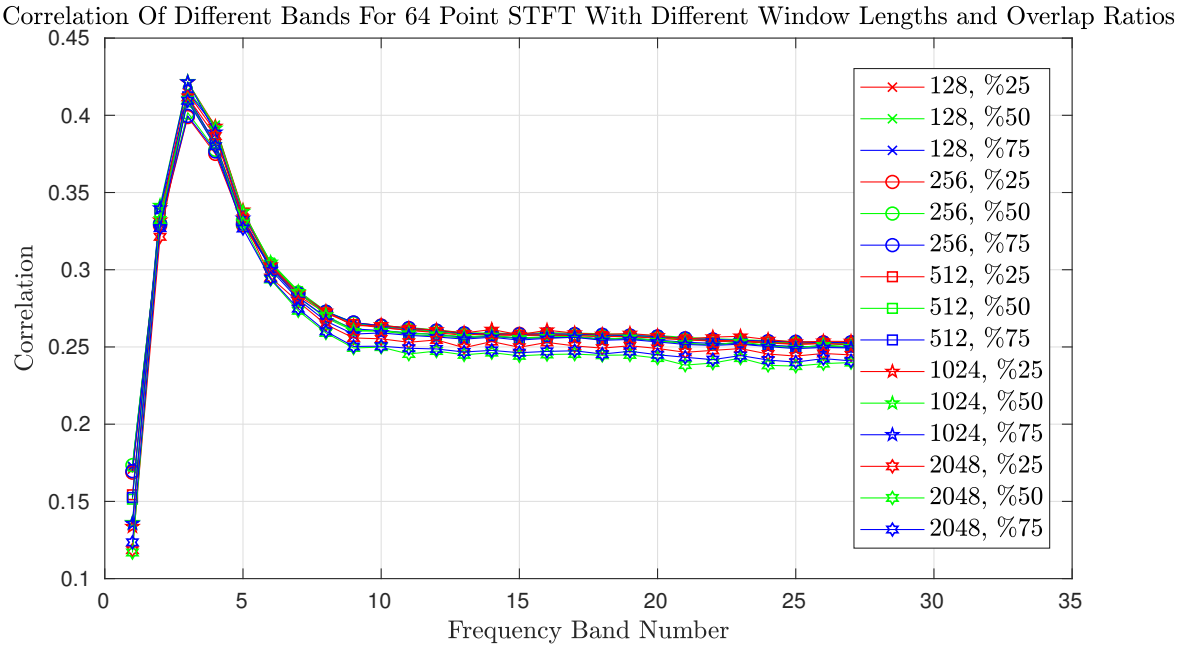

Figure 3.13. Mean of correlations for each band for STFT method with 64 fft bins, window lengths and overlap ratios

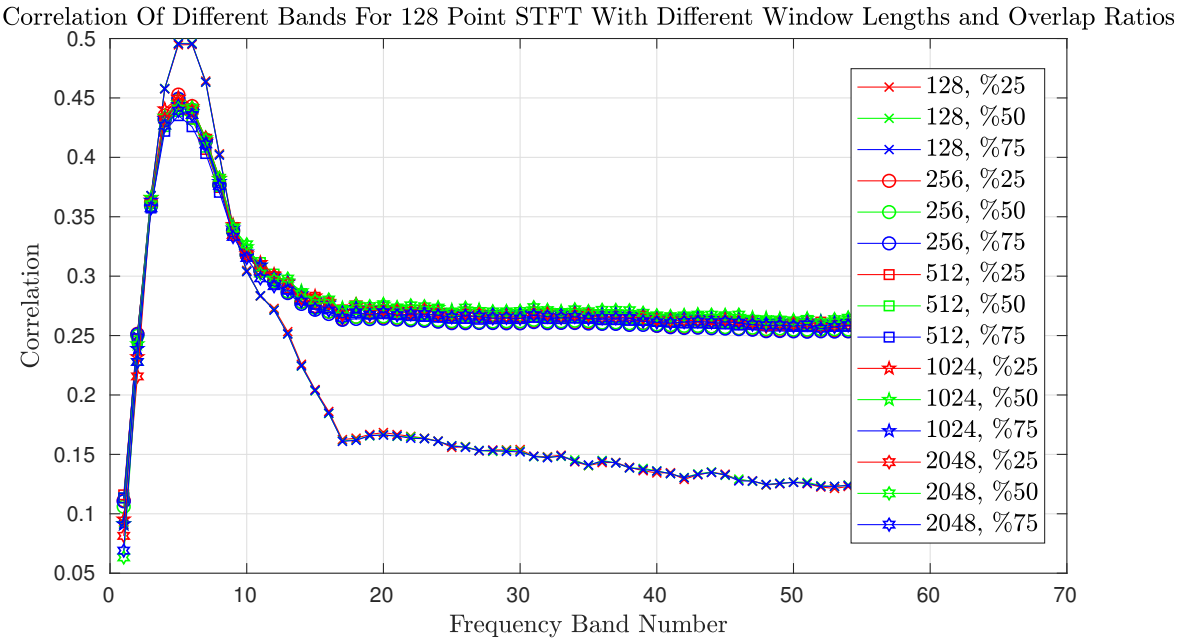

Figure 3.14. Mean of correlations for each band for STFT method with 128 fft bins, window lengths and overlap ratios

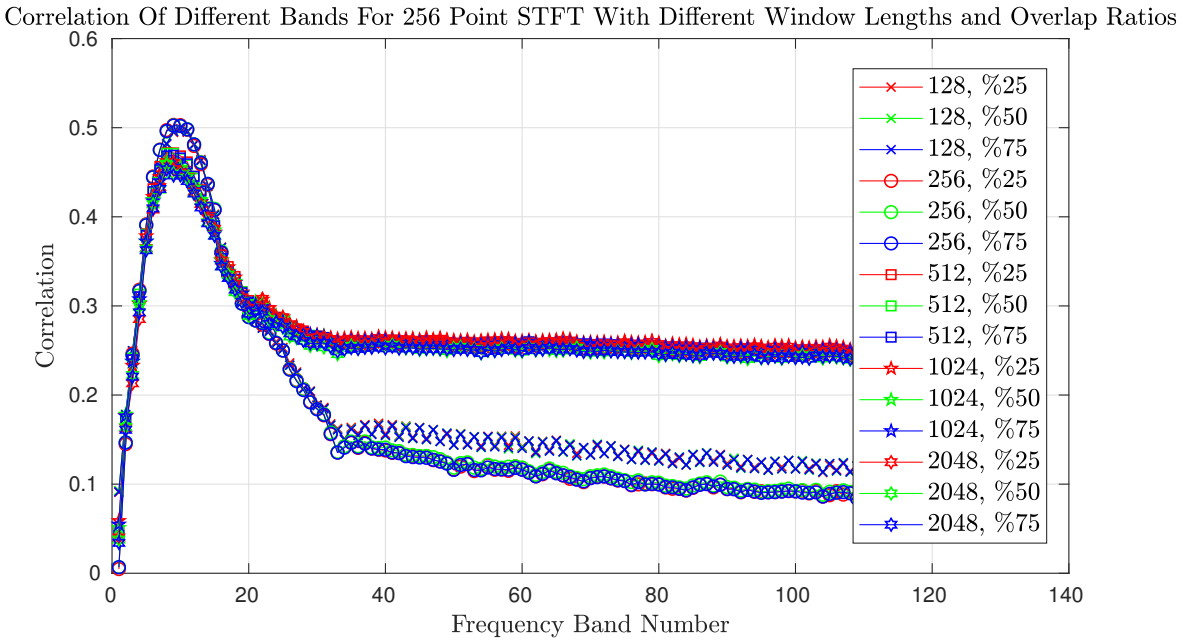

Figure 3.15. Mean of correlations for each band for STFT method with 256 fft bins, window lengths and overlap ratios

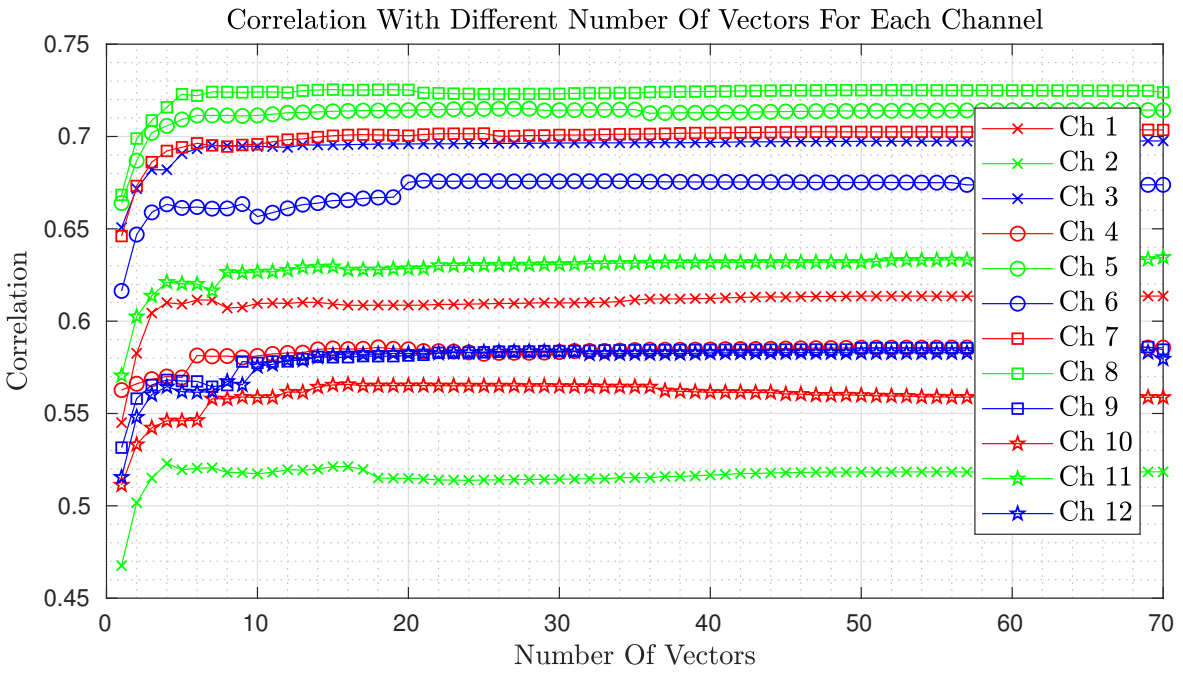

Figure 3.16. Mean of correlations for each channel with different number of vectors unified

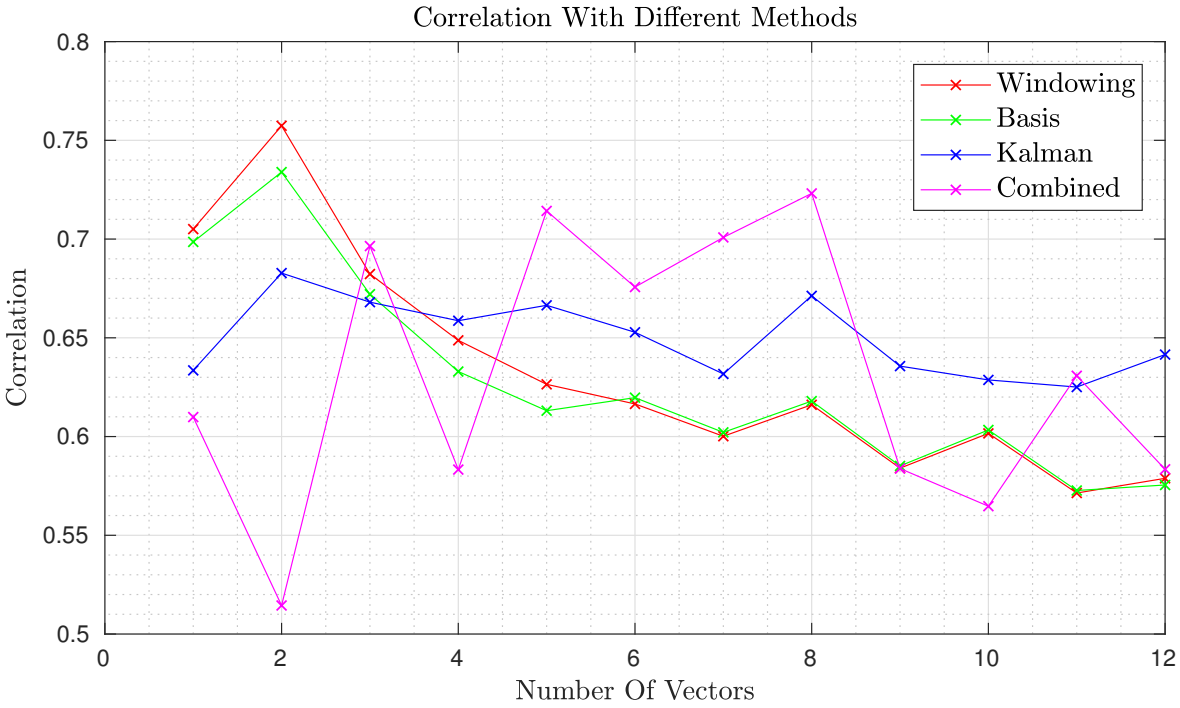

Figure 3.17. Mean of correlations for each channel with diffent methods

modeling, TVAR modeling with basis functions and TVAR modeling with Kalman filter respectively. There is not a significant difference among these three approaches. Average correlation coefficient of combined estimation with airflow is 0.63.

4. AIRFLOW PHASE ESTIMATION

In this chapter, more than one method are presented to estimate the respiratory phases. In one approach, the estimated airflow and in the other approach neural networks are used. In both methods the estimated breathing period is used.

4.1. Period Estimation

It is assumed that the period of breathing does not change abruptly and stays almost constant for each recording. In order to estimate the period, the autocorrelation function (ACF) of the absoulte airflow estimation is used. For a periodic wave, the ACF is also periodic with the same period and there are peaks at the integer products of the period. So, the period can be estimated by calculating the distances between the peaks. However, since the signal is noisy there are many local maxima, so instead of estimating the distance between peaks, we look at the ACF of ACF of the signal that is being analyzed, and use the location of the maximum of local peaks in the part that is determined by minimum and maximum period. The equation for estimated period is given in (4.1). A visual description of estimating the period is given in Figure 4.1.

$$T' = period_{min} + \arg\max(R_{R_x}[period_{min} : period_{max}]) \tag{4.1}$$

4.2. Phase Estimation With Neural Networks

A neural network is used to decide the phase of a given signal segment. The following features are used: AR coefficients, Shannon entropy estimate, percentile frequencies (f_{25}, f_{50}, f_{75} and f_{90}) and the ratio between each of them, variance, spectral magnitude and kurtosis. Range of these features change for each recording, bu the

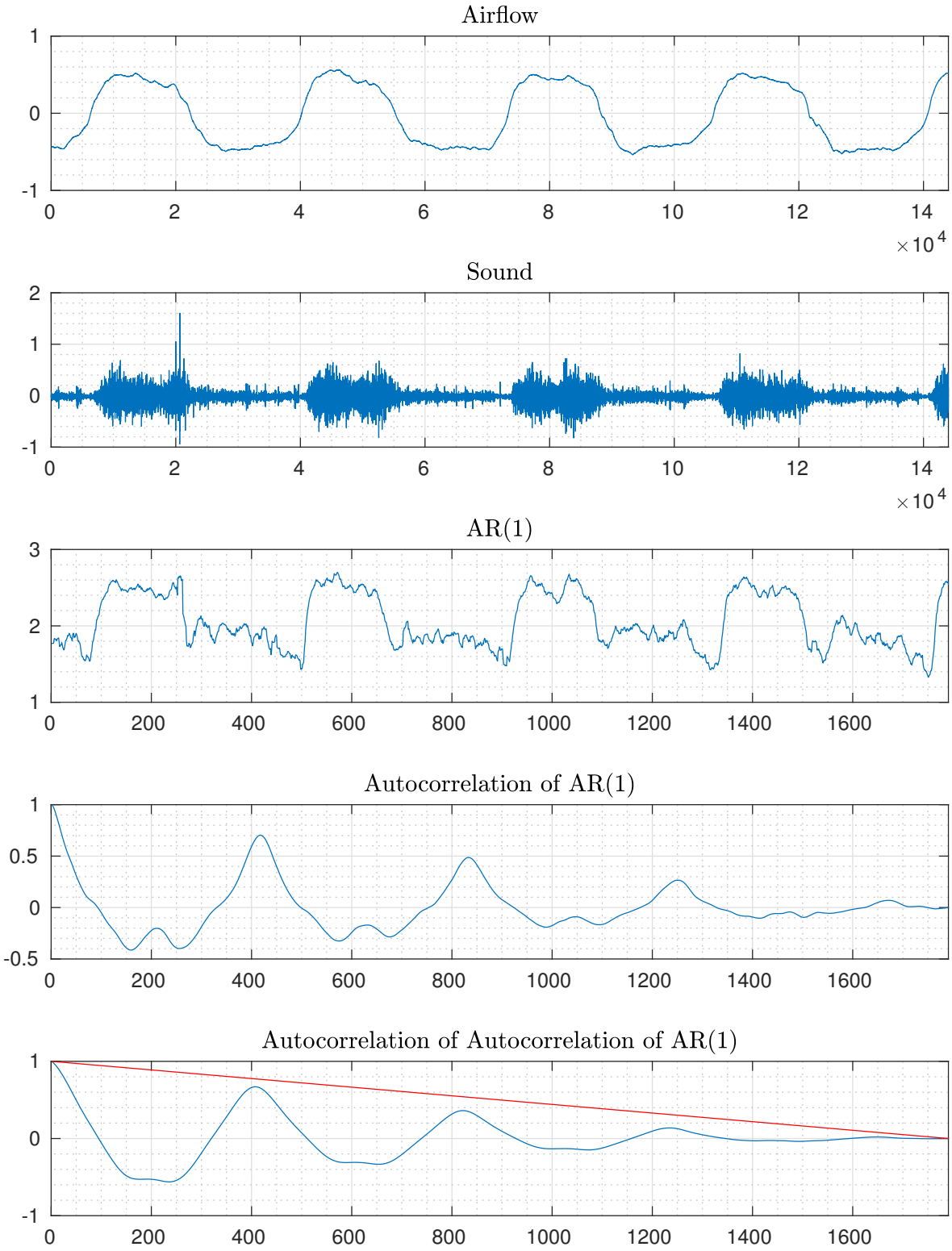

Figure 4.1. Visual Description Of Period Estimation

difference between inspiration and expiration does not change, so z-score is used before giving these features to neural network. The ratio of blue function to the red line at the end is taken into consideration.

4.2.1. Description of Neural Networks

A neural network is a function with many inputs and a single output. Formulation and development of neural networks are inspired from biological nervous system. Input values of a neural network is processed by dozens of interconnected functions, and these functions are called "neuron"s. A neuron can be thought as a function with multiple inputs and a single output. A neuron's output is determined by the activation function [19].

4.2.1.1. Neuron. Mathematical expression of a neuron's activation function is given in (4.2). Here β is the activation function. Activation function may be in several different forms. It is selected based on the application where the neural network is used and the distribution of input values. Activation functions are generally selected or constructed in a way that they are easily differentiable. Some of popular activation functions are given in Figure 4.3.

$$y = \beta(\sum_{i=1}^{N}(w_i x_i)) \tag{4.2}$$

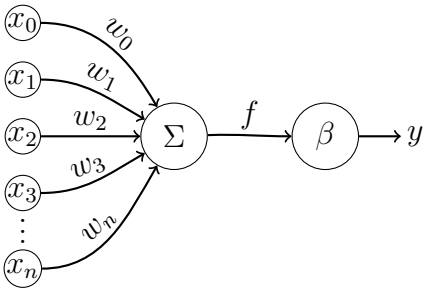

Figure 4.2. Diagram of A Neuron

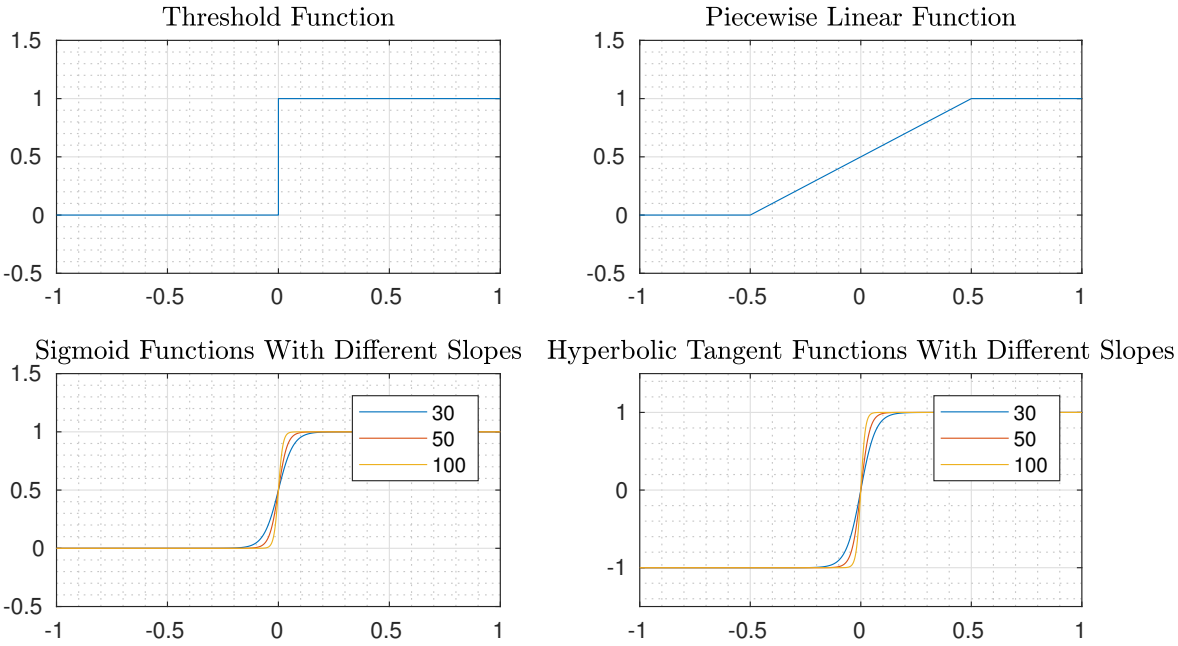

Figure 4.3. Some Activation Functions

4.2.1.2. Layers In Neural Networks. There are three different layers in neural networks, input layer, output layer and hidden layers. Input and output layers are where the input values are received and output values are given out respectively. Hidden layers are where the information from input layer or previous hidden layer is processed. Hidden layers may have arbitrary number of neurons and there may be any number of hidden layers in a neural network.

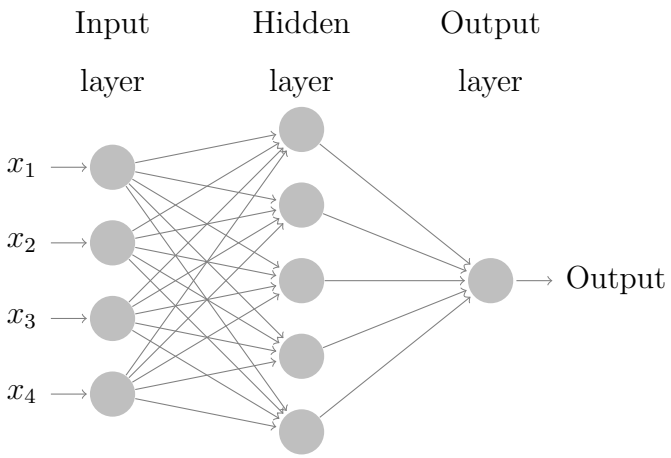

Figure 4.4. A Neural Network With One Hidden Layer

4.2.1.3. Learning Process In Neural Networks. Learning is the primary property of neural networks, it enables a neural network improve self performance.

The learning processes can be divided into three categories with respect to the learning paradigms. These categories are supervised, reinforcement and unsupervised learning. In supervised learning, the desired output so the error is known in the learning process. In reinforcement learning there is a performance measure which is being tried to be maximized. In unsupervised learning however, there is no desired output or performance measure available. We will use supervised learning since the correct phases are known to us.

Learning methods can be divided into four types, error-correction learning, memory based learning, Hebbian learning, competitive learning and Boltzmann learning. Error-correction learning is used in this study with an aim to minimize the total error measure by adjusting the synaptic weights.

4.2.2. Features

In this section, the features which are used in the neural network approach are presented. Each feature is calculated for all the sound samples. However while looking at features, one can see that the patterns do not change however the range of values changes. To overcome this issue each feature series from each sound gets normalized by using z-score. Z-score is the measure which indicates the distance a random sample has to its source mean. The formula for z-score is given in (4.3). For each sound sample and feature, the $\hat{\mu}_X$ and $\hat{\sigma}_X$ are calculated over all frames.

$$z_i = \frac{x_i - \hat{\mu}_X}{\hat{\sigma}_X} \tag{4.3}$$

The Kullback-Leibler (KL) divergence is also used to quantify how much the distributions for inspiration and expiration differ from each other for each feature. KL-divergence is a definition from information theory and it gives a distance between probability distributions. The formula for KL-divergence is given in (4.4) [20].

$$D_{KL}(p(x)||q(x)) = \sum_{x \in X} p(x) \log \frac{q(x)}{p(x)} \tag{4.4}$$

4.2.2.1. AR Coefficients. When the respiratory sounds are modeled as AR processes and the AR coefficients are obtained, it is seen that estimated AR coefficients behave differently for inspiration and expiration. As an example, for the case of the first AR coefficient it seems as the coefficients are attenuated for expiration phases. So it was decided to use AR coefficients as a feature to the neural network. A detailed explanation about AR models and methods to estimate AR coefficients is given in Section 3.

Distributions of AR coefficients during inspiration and expiration for the third channel are given in Figure 4.5

4.2.2.2. Shannon Entropy Estimate. Entropy is a measure which gives information about the complexity of the samples collected. As the randomness of the samples increases entropy also increases. The formula to calculate entropy is given in (4.5) [20]. In general we have a wider range for signal values in inspiration, so we expect entropy to be greater for the segments belonging to inspiration.

Distributions of Shannon's entropy estimates during inspiration and expiration for the third channel is given in Figure 4.6

$$H(X) = -\sum_{x \in X} p(x) \log(x) \tag{4.5}$$

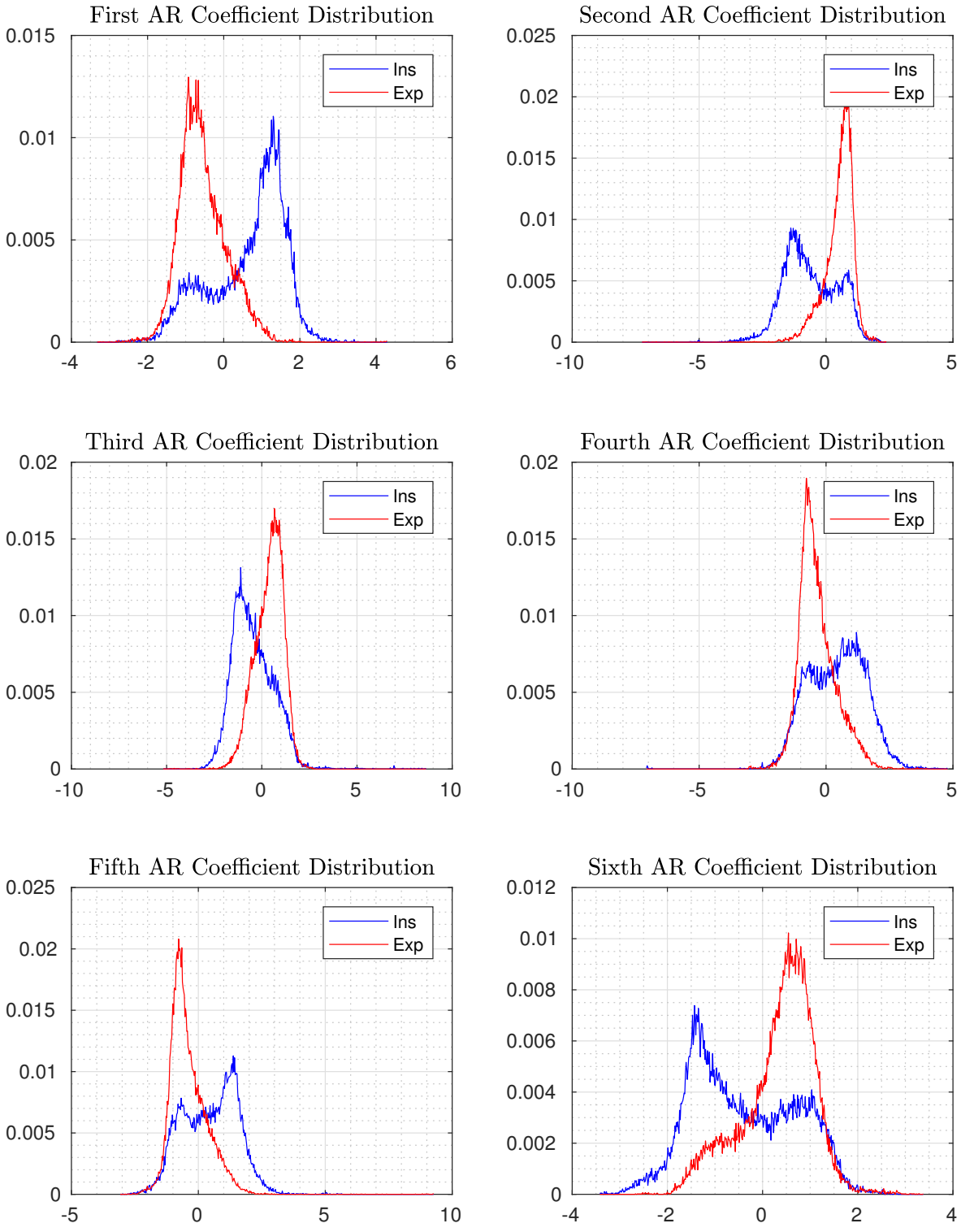

Figure 4.5. Distribution of AR Coefficients For Inspiration and Expiration

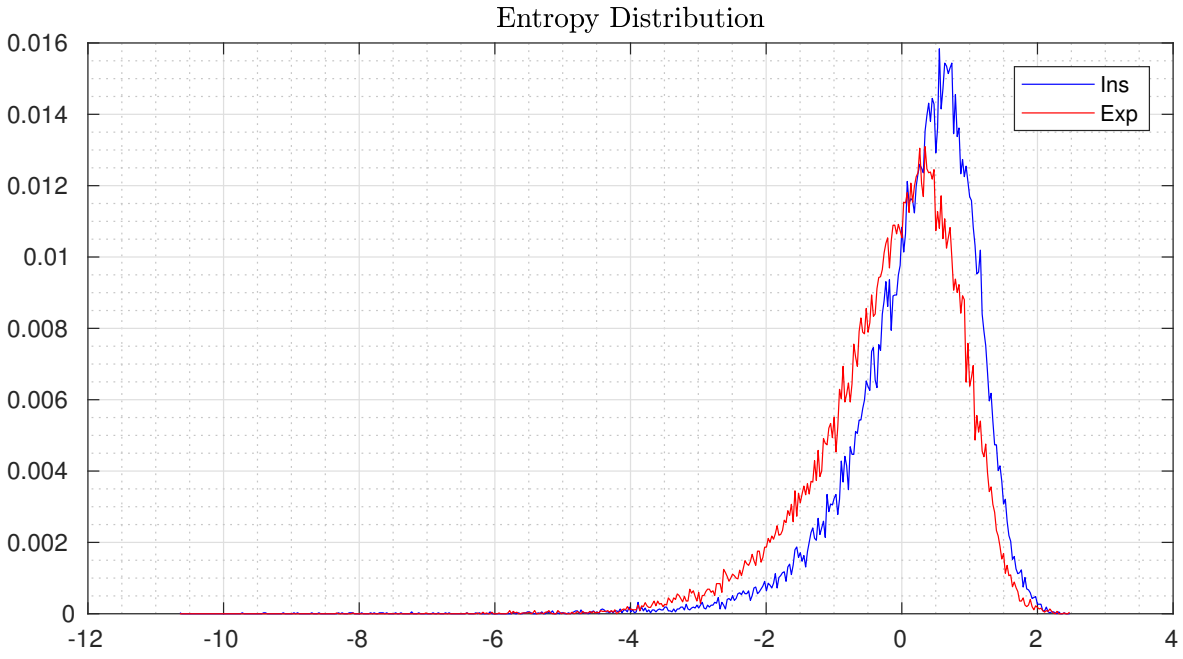

Figure 4.6. Distribution of Shannon Entropy Estimate For Inspiration and Expiration

4.2.2.3. Percentile Frequencies. A percentile frequency is the frequency at which the cumulative sum of power spectral density is equal to the defined percent of total power. In order to calculate these frequencies, first the power spectral density, $P_{XX}(f)$, is estimated according to the formula in (4.8), where $x(t)$ is the signal in time domain, $X(f)$ is the Fourier transform of $x(t)$. Percentile frequencies and their relations are measures which are widely used in respiratory signal analysis [21, 22]. Since the expiration and inspiration phases have different time-frequency content, percentile frequencies may be used as input to classifier neural network. Definition of a percentile frequency, f_y, is given in (4.8).

Distributions of percentile frequencies and their ratios between each other during

inspiration and expiration for third channel is given in Figure 4.7.

$$X(f) = \int_{-\infty}^{\infty} x(t) e^{-2\imath f t \pi} dt \tag{4.6}$$

$$P_{XX}(f) = X(f)^2 \tag{4.7}$$

$$f_y = \arg\min_x \frac{\int_0^x P_{XX}(f) df}{\int_0^\infty P_{XX}(f) df} > \frac{y}{100} \tag{4.8}$$

4.2.2.4. Variance. Variance corresponds to power and observations show that power for different respiratory phases differs. So we decided to use variance as a supportive feature. Sample variance is calculated as in (4.10).

Distributions of variance of windows during inspiration and expiration for the third channel are given in Figure 4.7.

$$\hat{\mu}_X = \frac{\sum_{x \in X} x}{|X|} \tag{4.9}$$

$$\hat{\sigma}_X^2 = \frac{\sum_{x \in X} (x - \hat{\mu}_X)^2}{|X| - 1} \tag{4.10}$$

4.2.2.5. Spectral Magnitude. The magnitudes of several frequency bands are calculated for each segment using FFT. The spectral band's magnitude are calculated by taking FFT of windows after multiplying them with a Hamming window for smoothing. 128 points FFT is used and each band represents a band of 75 Hz. We used the following bands' magnitudes: {75 Hz-150 Hz, 150 Hz-225 Hz, 225 Hz-300 Hz, 300 Hz-375 Hz, 375 Hz-450 Hz}.

Distributions of spectral magnitudes of windows during inspiration and expiration

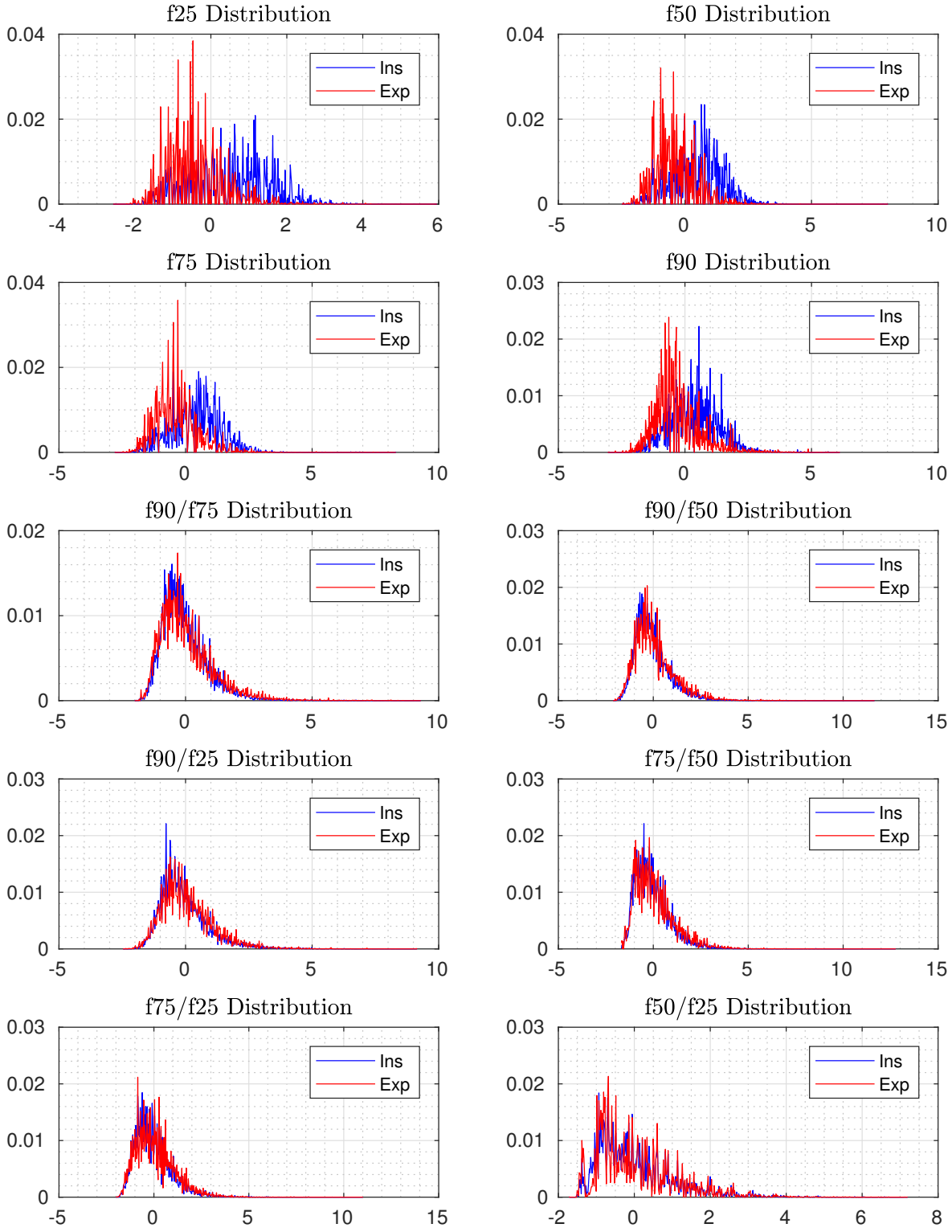

Figure 4.7. Distribution of Percentile Frequency Measures For Inspiration and Expiration

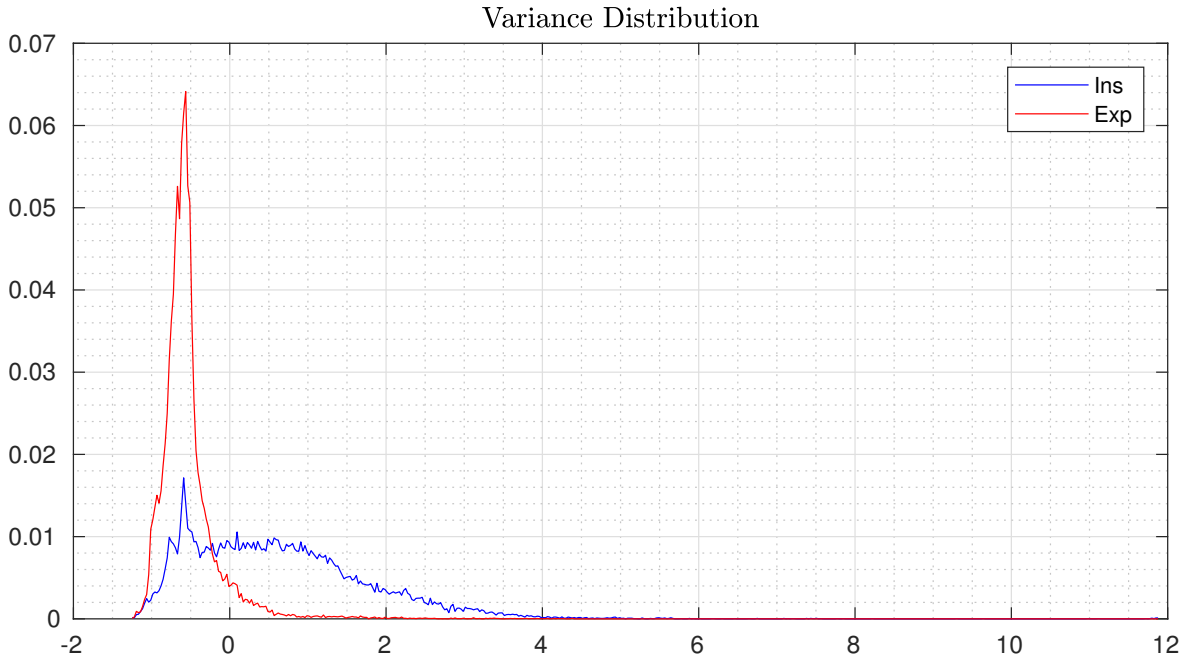

Figure 4.8. Distribution of Variance For Inspiration and Expiration

for the third channel are given in Figure 4.9.

4.2.2.6. Kurtosis. Kurtosis is the ratio of the fourth moment to square of second moment. It is a statistical feature which has been used in respiratory signal analysis. Formula for kurtosis is given in (4.11)

Distributions of kurtosis of windows during inspiration and expiration for the third channel are given in Figure 4.10.

$$\bar{K} = |X| \frac{\sum_{x \in X} (x - \hat{\mu}_X)^4}{(\sum_{x \in X} (x - \hat{\mu}_X)^2)^2} \tag{4.11}$$

The average KL-divergence for features is given in Figure 4.11. The feature indices are consistent with the order features as explained above.

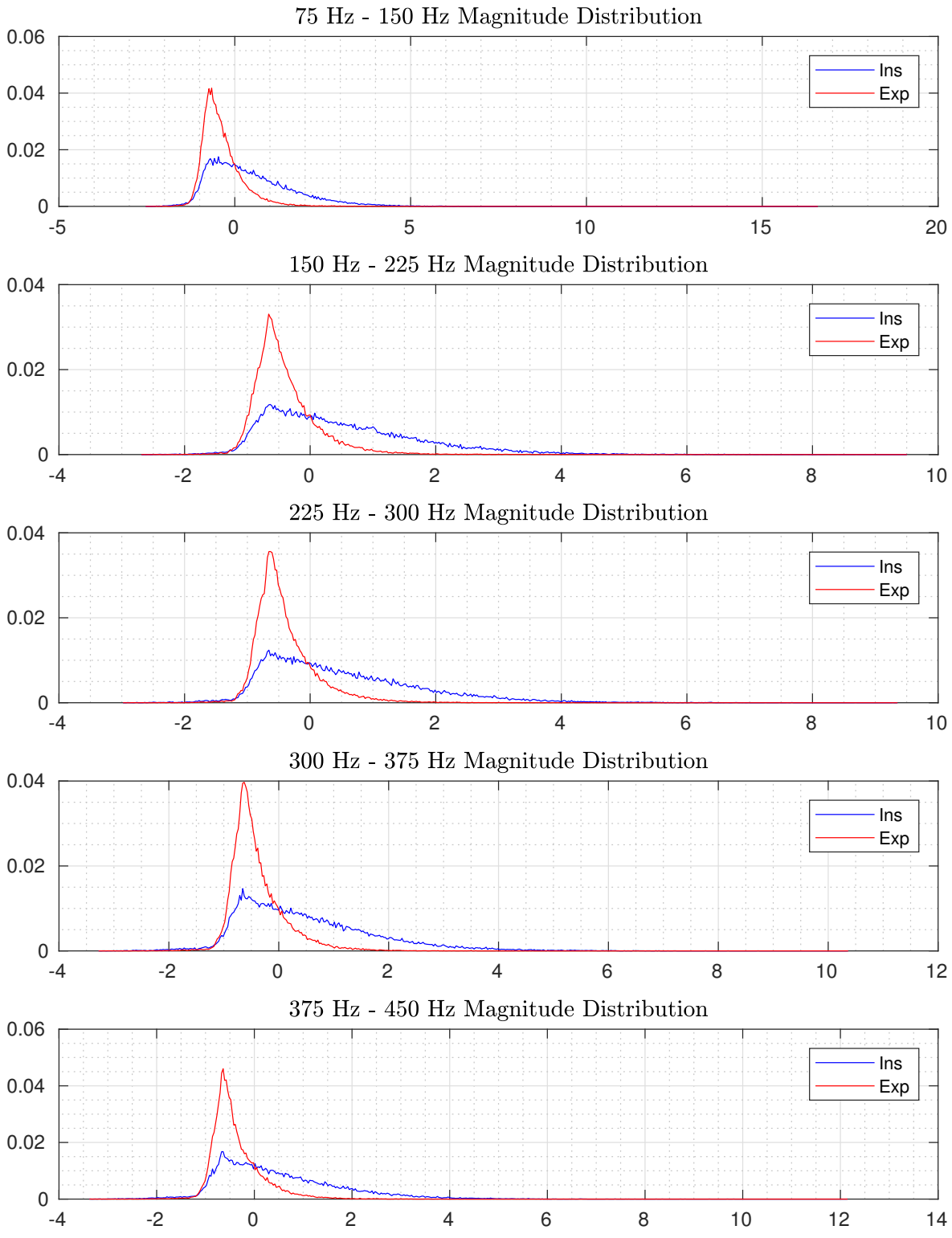

Figure 4.9. Distribution of Spectral Magnitudes For Inspiration and Expiration

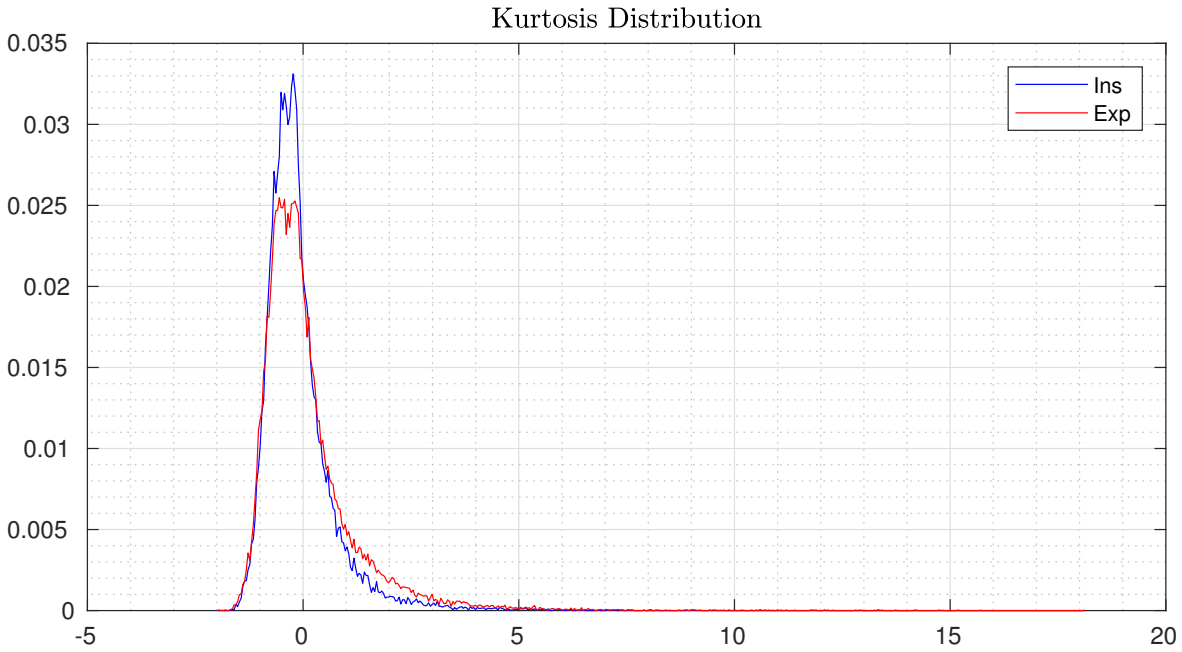

Figure 4.10. Distribution of Kurtosis For Inspiration and Expiration

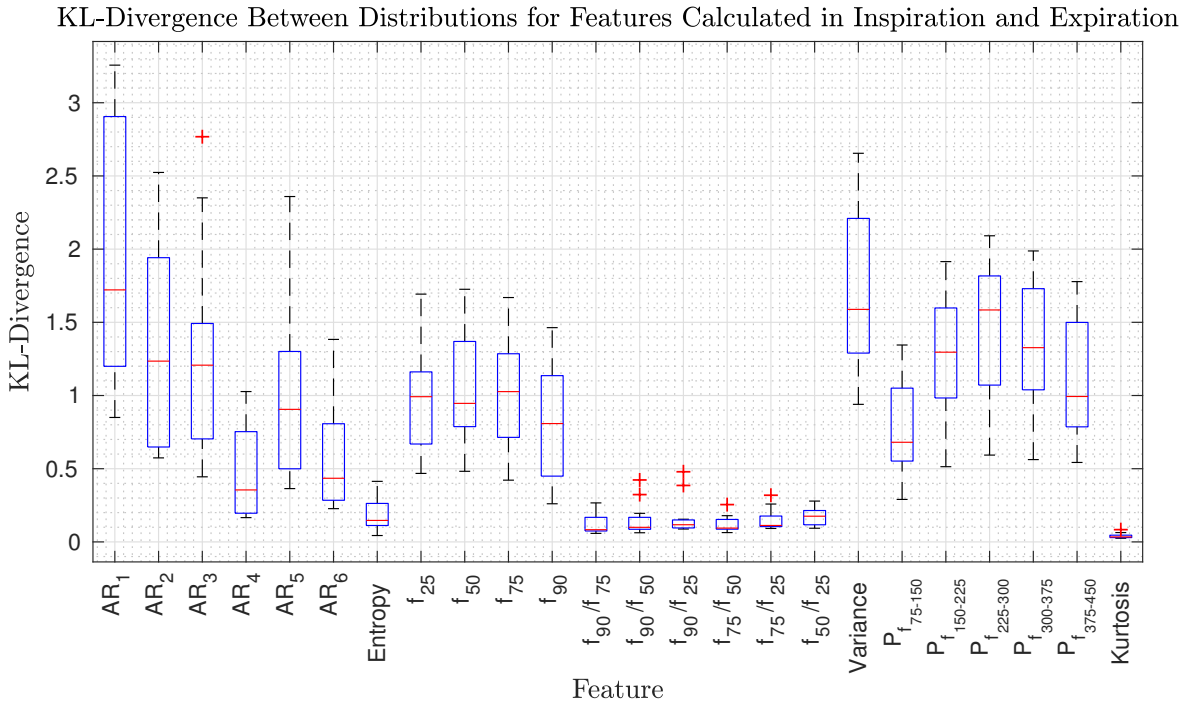

Figure 4.11. KL-Divergence Between Distributions for Features Calculated in Inspiration and Expiration

4.2.3. Denoisining The Output of Neural Network

The output of neural network is not very good in terms of estimating the phase correctly and it alternates too much even in short durations. In order to overcome this problem, a filtering is needed. Linear filters do not perform well since they display many discontiunities, so it is decided to use a filter that takes the contiunity into account and since the period was estimated earlier, it was used for filtering purposes. A periodic square wave is created with the period equal to the the estimated period and with 50% duty cycle. The cross correlation between this square wave and the output of neural network is calculated. This indicates the required amount of shift that is needed for the square wave to fit on to the phase of airflow. It must be noted that the airflow is assumed to be periodic and that its duty cycle is 50%.

4.3. Phase Estimation With Estimated Airflow Curve

The airflow phase curve is estimated using the estimated airflow curves. In order to do that, the estimation which has the most correlation with the absolute airflow curve is used, so the first AR coefficient of consecutive and overlapping windows is used. It is reported that the onsets can be found by looking at local minima of estimated absolute airflow curve. In this case, local minima analysis only didn't solve the problem so some heuristic algorithms based on observations were developed.

4.3.1. Prefiltering

In trying to locate the local minima, because of the noisy nature of estimated airflow, there are many false minima. To overcome this problem a median and moving average filter are applied. A median filter is chosen to filter out the spikes and a moving average filter to smooth the signal. Describing formulae for median and moving average filters with $2K+1$ taps are given in (4.12) and (4.13). In this study 25 taps for median

filter and 35 taps for moving average filter are used.

$$y_i = \text{med}(x_{\max(0,i-K)}, x_{\max(0,i-K+1)}, ...x_i, ..., x_{\min(L,i+K-1)}, x_{\min(L,i+K)}) \tag{4.12}$$

$$y_i = \frac{\sum_{j=\max(0,i-K)}^{\min(L,i+K)} x_j}{\min(L, i+K) - \max(0, i-K) + 1} \tag{4.13}$$

. A figure showing unfiltered and filtered signal is depicted in Figure 4.12

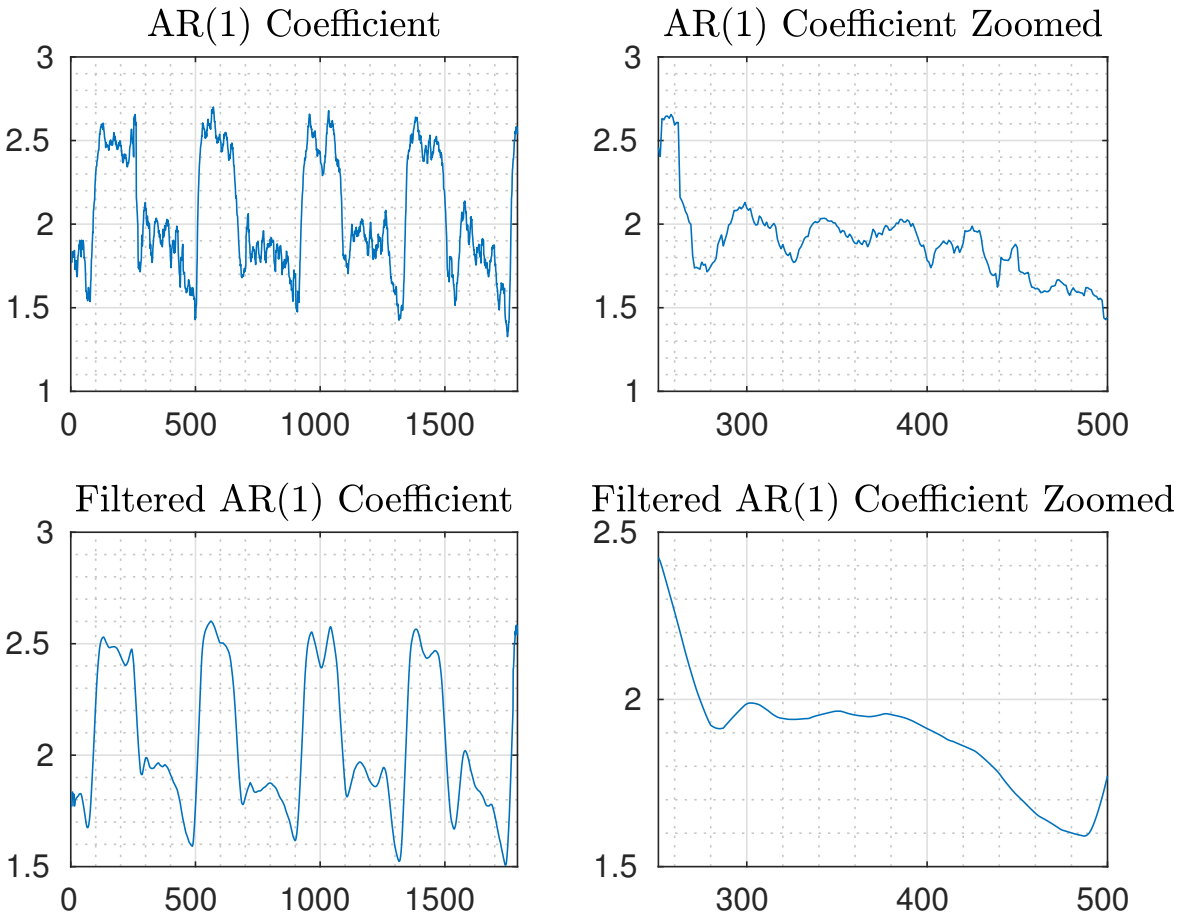

Figure 4.12. Filtering The Flow Estimate

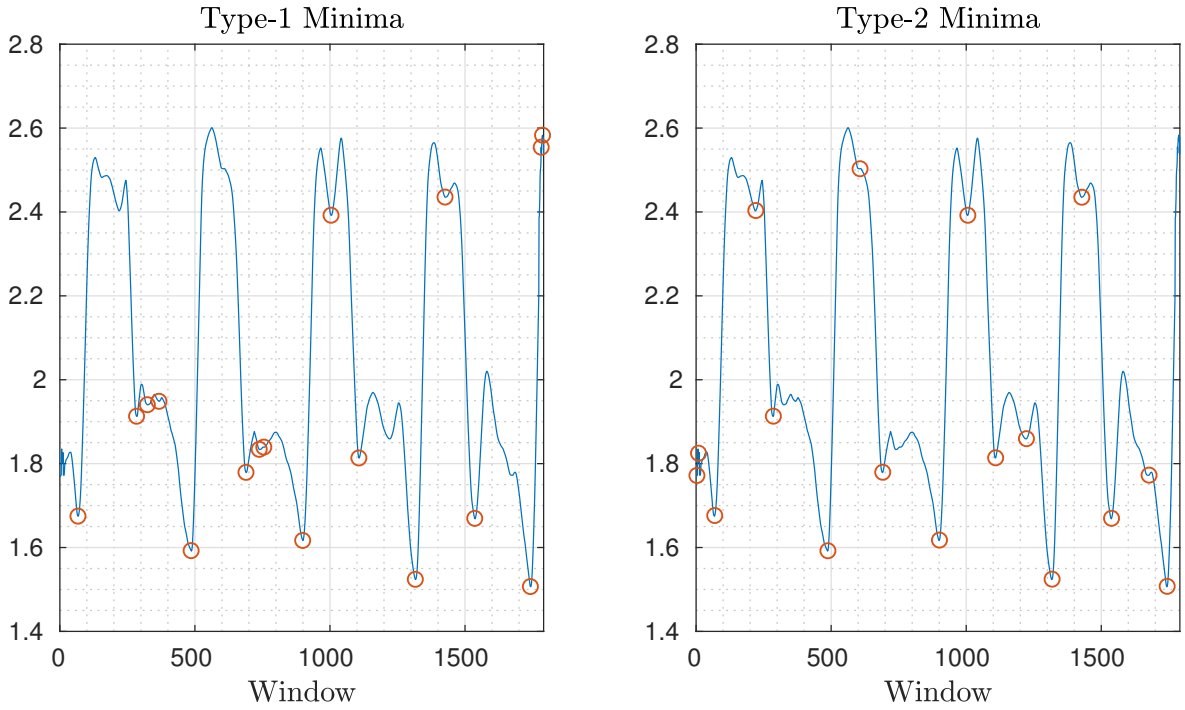

Figure 4.13. Type-1 and Type-2 Minima

4.3.2. Local Minima Extraction

The number of local minima is decreased by filtering, however, there are still too many minima to process. So, a heuristic algorithm is added for the selection of local minima. Two types of local minimum are used: one type, *type*-1, is mostly seen in transitions from expiration to inspiration and the other, *type*-2, is mostly seen in transitions from inspiration to expiration. The examples of *type*-1 and *type*-2 minima are shown in figure 4.13.

- *Type*-1 Minimum: A minimum smaller than all minima in its right neighborhood.
- *Type*-2 Minimum: A minimum smaller than all minima in its left neighborhood.

4.3.3. Selection of Transition Points

The period estimation and local minima are together used to decide on the location of transition points. While all the local minima are candidate transition points, it

is assumed that the distribution of the distances between consecutive transitions from inspiration to expiration and expiration to inspiration have a distribution with a small variance and a mean which is equal to the period estimation. So, first, the number of transitions in each direction is decided on. Then all the subsets of local minima whose cardinality is equal to the number of transitions are listed and the differences between adjacent elements are calculated. Finally the likelihoods of each subset are calculated according to (4.14) and the one which has highest likelihood is selected. After selecting the first transition points set, in order to decide on the set belonging to the other transition type, we also look at the distance to the set of first transition type. In this no assumption is made on the value of the duty cycle. A block diagram explaining the procedure is given in Figure 4.14. An example of change point estimation is given in Figure 4.15.

$$L(\vec{d}) = \frac{\exp((\vec{d} - T')^T(\vec{d} - T')/\sigma^2)}{\sigma} \tag{4.14}$$

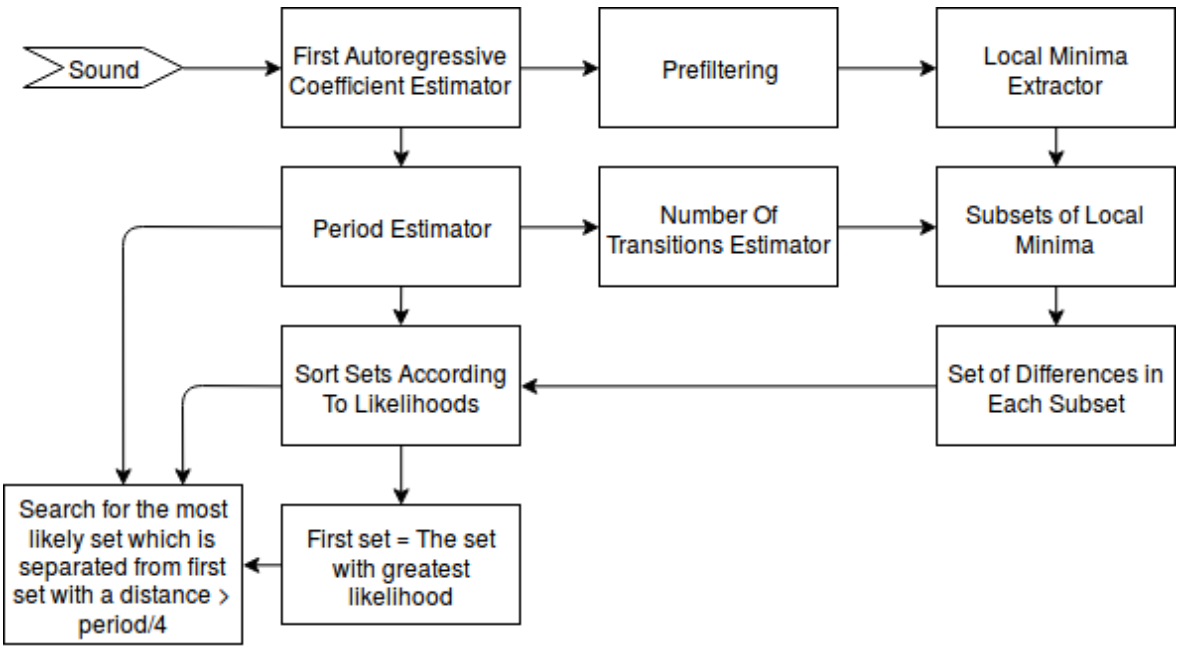

Figure 4.14. Block Diagram Explaining the Transition Point Estimation

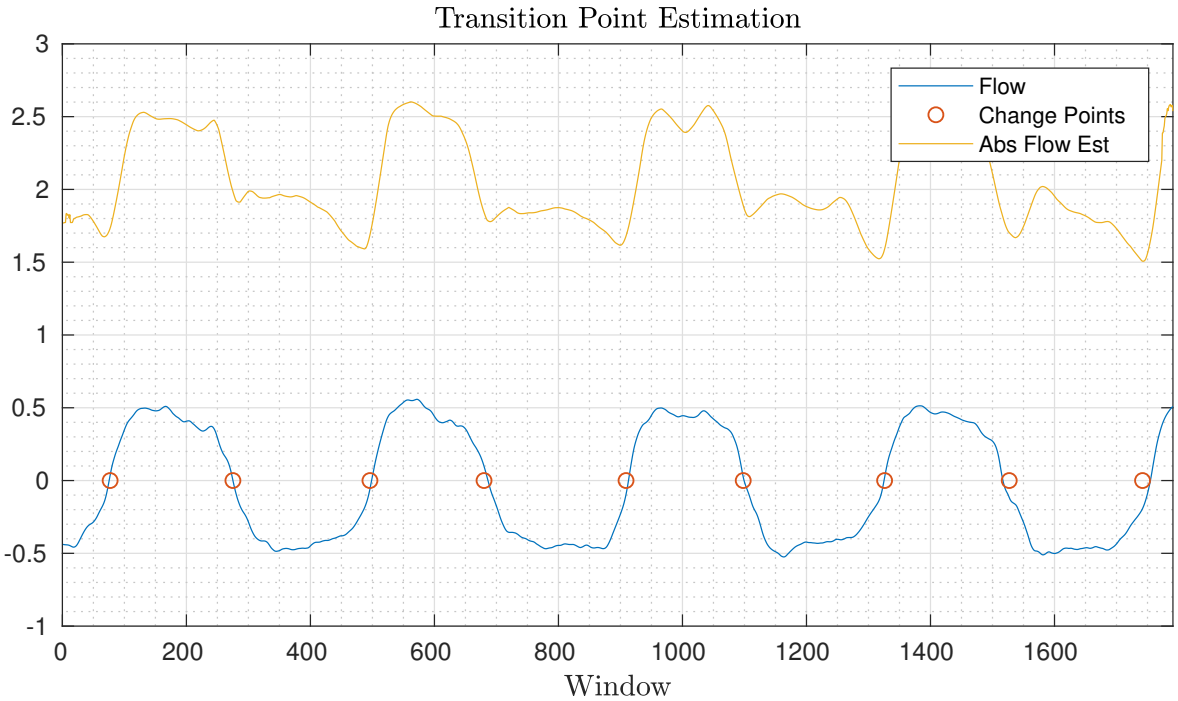

Figure 4.15. Transition Point Estimation

4.3.4. Estimating The Phases Given Transition Points

The phases of segments are estimated after deciding on transition points by using the first AR coefficient of segments divided by the transitions points. Two groups are created and each group includes nonconsecutive segments. Then the AR coefficients for each segment are calculated, and the group with a greater average AR coefficient is labeled as inspiration. This method works with a success rate of 96%.

4.4. Experiments & Results

4.4.1. Neural Networks

Matlab's neural network toolbox is used in the training process. The performance function is selected to be cross-entropy since it is a standard performance function used for classification purposes and training function is selected to be scaled conjugate gradient. Neural networks with different number of hidden neurons are used and it is

observed that the correlation between neural network's output and phase type does not change significantly with the number of hidden neurons. This experiment is carried out on the third channel of 10 subjects. The boxplot showing results for different number of hidden neurons is given in Figure 4.16. It is decided to use 20 neurons.

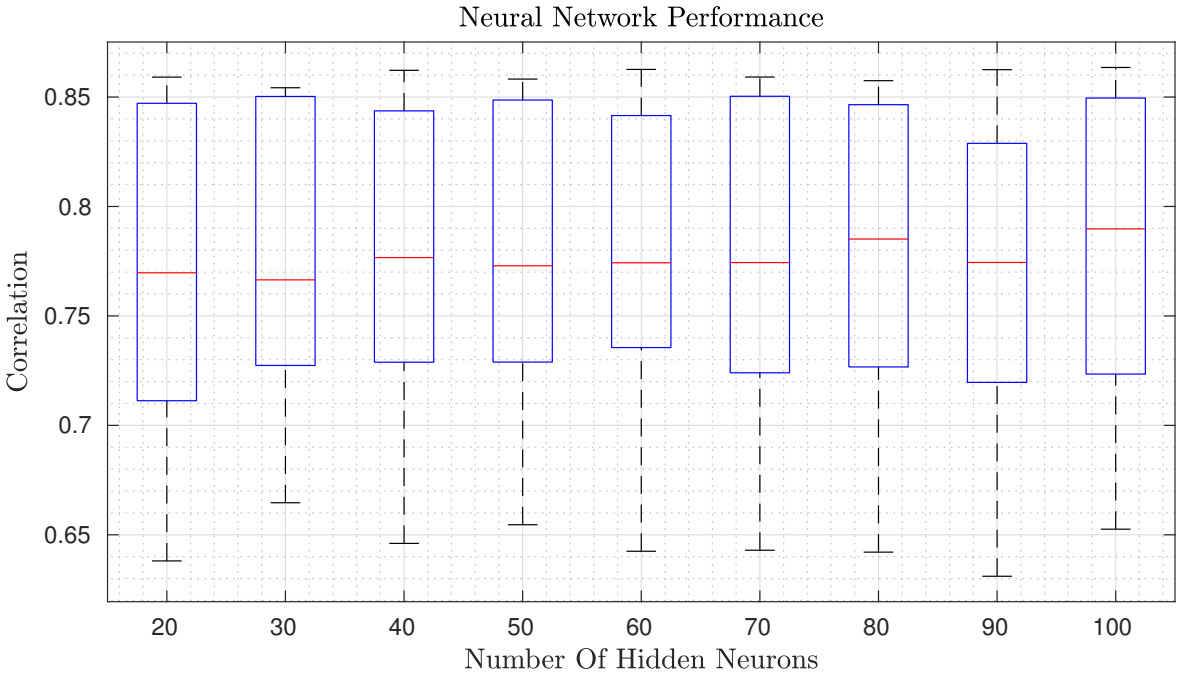

Figure 4.16. Performance of Neural Network vs Number of Hidden Neurons

The performance of neural networks is measured by using correlation measure. The boxplot of correlations between neural network's output and the phase is given in Figure 4.17. Then the output of neural networks is corrected by using the period information, and the result is shown in Figure 4.18.

In addition to correlation measure the deviation of detected transition points from real transition points is also measured. A deadband which is equal to 5% of peak-to-peak voltage around zero is introduced before calculating the true transition points.

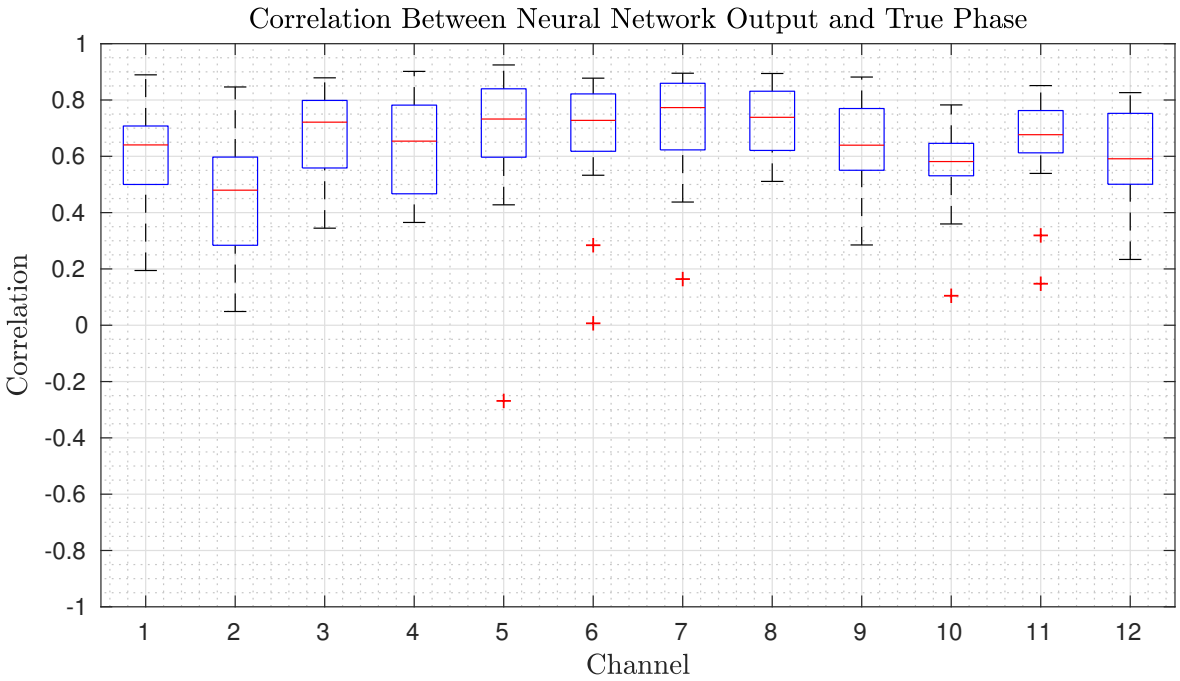

Figure 4.17. Performance of Neural Network vs Channels

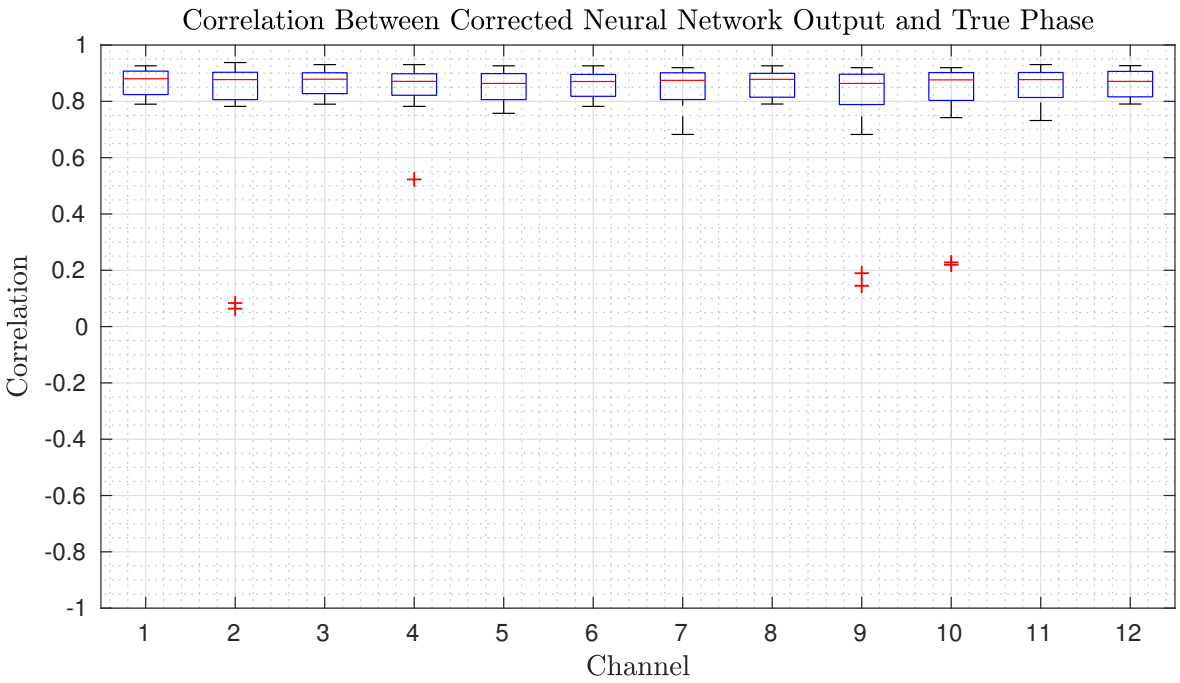

Figure 4.18. Performance of Neural Network vs Channels After Correction

Table 4.1. Deviation From True Transitions in Milliseconds and Error in Percentage

Channel	1	2	3	4	5	6	7	8	9	10	11	12	Avg
Ins to Exp	74	183	76	87	77	74	80	71	146	115	86	82	97
Error/Exp %	4.3	10.6	4.4	5.0	4.5	4.3	4.6	4.1	8.5	6.7	5.0	4.8	5.6
Error/Tot %	2.4	5.8	2.4	2.8	2.4	2.4	2.5	2.3	4.6	3.6	2.7	2.6	3.0
Exp to Ins	64	150	66	77	63	67	62	65	126	123	68	65	83
Error/Ins %	4.4	10.4	4.6	5.4	4.4	4.7	4.3	4.5	8.8	8.6	4.7	4.5	5.8
Error/Tot %	2.0	4.8	2.0	2.4	2.0	2.1	2.0	2.0	4.0	3.9	2.1	2.1	2.6

4.4.2. Transition Points Detection Based On Local Minima

The first AR coefficient and period information are used to estimate the transition points and calculated the first AR coefficient of the segments between transition points are calculated to decide on phase. The correlation between estimated and true flow phase is given in Figure 4.19 and the deviation from true transitions is given in Table 4.2.

Table 4.2. Deviation From True Transitions in Milliseconds and Error in Percentage

Ch	1	2	3	4	5	6	7	8	9	10	11	12	Avg
I to E	112	121	130	110	96	117	159	102	88	176	110	118	120
Err/Exp	6.5	7.0	7.6	6.4	5.6	6.8	9.3	5.9	5.1	10.2	6.4	6.9	7.0
Err/Tot	3.5	3.8	4.1	3.5	3.0	3.7	5.0	3.2	2.8	5.6	3.5	3.7	3.8
E to I	106	186	94	198	113	117	157	149	104	143	131	131	131
Err/Ins	7.4	12.9	6.5	13.8	7.9	8.1	10.9	10.4	7.2	10.0	9.1	9.1	9.1
Err/Tot	3.4	5.9	3.0	6.3	3.6	3.7	5.0	4.7	3.3	4.5	4.2	4.2	4.1

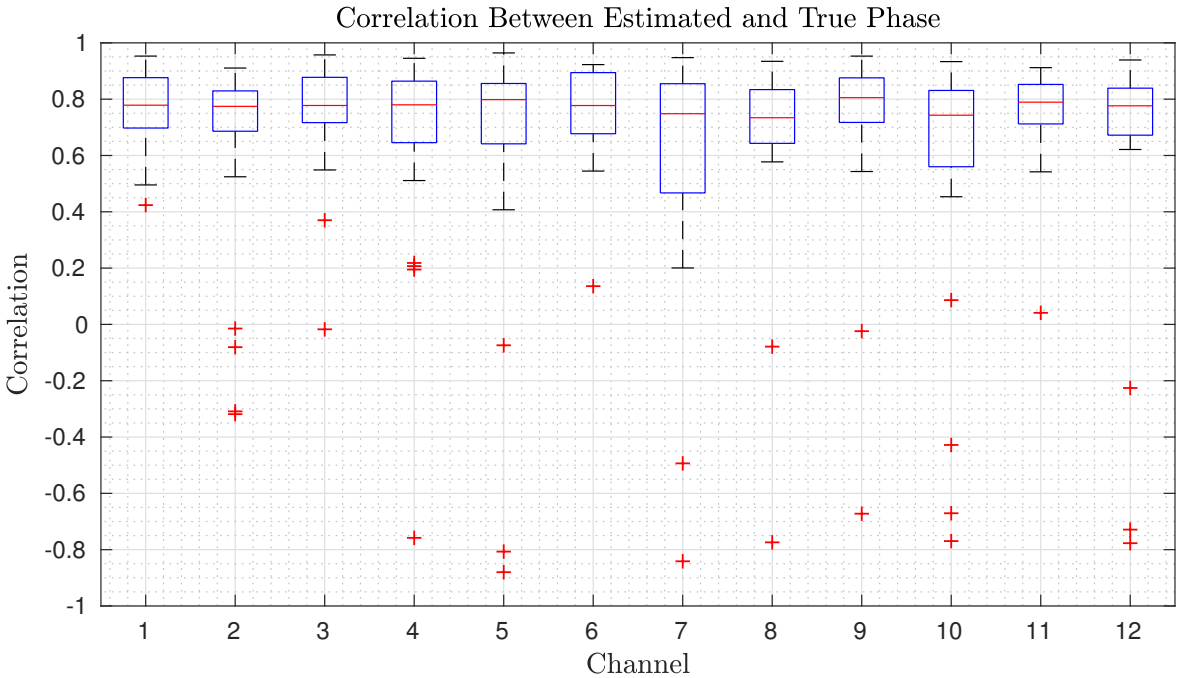

Figure 4.19. Performance of Phase Estimation Based On Local Minima

5. CONCLUSION

In this thesis, methods, including some from literature, are suggested and tested to estimate the curve and phase of the airflow at the mouth by using the sounds recorded on the chest wall. The respiratory airflow and phase information has diagnostic value, so their accurate estimation may increase pulmonary disease diagnosis performance using auscultation in case there is no airflow measurement.

In chapter 3, the TVAR modeling of respiratory sounds approach after a description of AR and TVAR processes is tested. The method in [11] which uses the basis functions to estimate the TVAR coefficients, the windowing based AR modeling and Kalman filter for TVAR modeling approaches are also implemented in this thesis and the performance is measured by looking at the correlation coefficient between estimation and absolute value of airflow. From the results, it can be said that, all three approaches have similar performances. Later, the correlation of magnitudes of different frequency bands with the airflow itself is tested. Finally, the Wiener filter approach is introduced to unify different estimations of airflow.

In chapter 4, first, a method to estimate the period of breathing from the estimation of airflow, which is based on the first AR coefficient is given. Then, a neural network for classification of inspiration and expiration is used. The histograms of features (AR, Time-Frequency, Percentile Frequencies, Variance, Entropy and Kurtosis) from inspiration and expiration parts are presented consequently. A method to denoise the output of neural networks by using the period information and assuming a 50% duty cycle is presented. It is also tried to estimate the transition points by using the absolute airflow estimation and the period information.

In conclusion, the relation between respiratory sounds, their features and the airflow are investigated throughout this thesis. It can be concluded that, the phase

information can be extracted from respiratory sounds with a good performance by using the techniques in chapter 4 and the airflow curve can be estimated with the techniques in chapter 3 and that phase estimation performs better than airflow curve estimation.

REFERENCES

1. Sen, I., *Multivariate Modeling and Diagnostic Classification of Pulmonary Sounds*, Ph.D. Thesis, Bogazici University, 2013.

2. Gavriely, N., *Breath Sounds Methodology*, CRC Press, 1995.

3. H Pasterkamp, S. K. and G. Wodicka, "Respiratory sounds. Advances beyond the stethoscope.", *American Journal of Respiratory and Critical Care Medicine*, Vol. 157, pp. 974–987, 1997.

4. Sen, I., M. Saraclar and Y. P. Kahya, "A Comparison of SVM and GMM-Based Classifier Configurations for Diagnostic Classification of Pulmonary Sounds", *IEEE Transactions on Biomedical Engineering*, Vol. 62, No. 7, pp. 1768–1776, July 2015.

5. Yeginer, M., K. Ciftci, U. Cini, I. Sen, G. Kilinc and Y. P. Kahya, "Using lung sounds in classification of pulmonary diseases according to respiratory subphases", *The 26th Annual International Conference of the IEEE Engineering in Medicine and Biology Society*, Vol. 1, pp. 482–485, September 2004.

6. Lessard, C. S. and W. C. Wong, "Correlation of Constant Flow Rate with Frequency Spectrum of Respiratory Sounds When Measured at the Trachea", *IEEE Transactions on Biomedical Engineering*, Vol. BME-33, No. 4, pp. 461–463, April 1986.

7. Yadollahi, A. and Z. Moussavi, "Robust Respiratory Flow Estimation Using Statistical Properties of Tracheal Sounds", *2005 IEEE Engineering in Medicine and Biology 27th Annual Conference*, pp. 1106–1109, January 2005.

8. Huq, S. and Z. Moussavi, "Acoustic breath-phase detection using tracheal breath sounds", *Medical & Biological Engineering & Computing*, Vol. 50, No. 3, pp. 297–

308, March 2012, https://doi.org/10.1007/s11517-012-0869-9.

9. Moussavi, Z. K., M. T. Leopando, H. Pasterkamp and G. Rempel, "Computerised acoustical respiratory phase detection without airflow measurement", *Medical and Biological Engineering and Computing*, Vol. 38, No. 2, pp. 198–203, March 2000, https://doi.org/10.1007/BF02344776.

10. Golabbakhsh, M., Z. Moussavi and M. Aboofazeli, "Respiratory Flow Estimation from Tracheal Sound by Adaptive Filters", *2005 IEEE Engineering in Medicine and Biology 27th Annual Conference*, pp. 4216–4219, January 2005.

11. Ciftci, K. and Y. P. Kahya, "Respiratory airflow estimation by time varying autoregressive modeling", *2008 30th Annual International Conference of the IEEE Engineering in Medicine and Biology Society*, pp. 347–350, August 2008.

12. Sen, I. and Y. P. Kahya, "A Multi-Channel Device for Respiratory Sound Data Acquisition and Transient Detection", *2005 IEEE Engineering in Medicine and Biology 27th Annual Conference*, pp. 6658–6661, January 2005.

13. Shanmugan, K. and A. M. Breipohl, *Random Signals: Detection, Estimation, and Data Analysis*, Wiley, 1988.

14. de Hoon, M., T. van der Hagen, H. Schoonewelle and H. van Dam, "Why Yule-Walker should not be used for autoregressive modelling", *Annals of Nuclear Energy*, Vol. 23, No. 15, pp. 1219 – 1228, 1996, http://www.sciencedirect.com/science/article/pii/0306454995001263.

15. Haykin, S., *Kalman Filtering and Neural Networks*, Wiley, 1988.

16. Tary, J. B., R. H. Herrera and M. van der Baan, "Time-varying autoregressive model for spectral analysis of microseismic experiments and long-period volcanic events", *Geophysical Journal International*, Vol. 196, No. 1, pp. 600–611, January

2014.

17. Allen, J., "Short term spectral analysis, synthesis, and modification by discrete Fourier transform", *IEEE Transactions on Acoustics, Speech, and Signal Processing*, Vol. 25, No. 3, pp. 235–238, June 1977.

18. Haykin, S., *Adaptive Filter Theory*, Prentice-Hall Inc., 1996.

19. Haykin, S., *Neural Networks*, Prentice-Hall Inc., 2005.

20. Cover, T. M. and J. A. Thomas, *Elements Of Information Theory*, Wiley, 2006.

21. Aydore, S., *Wheeze Detection in Respiratory Sounds via Statistical Signal Modeling*, Master's Thesis, Bogazici University, 2009.

22. Sankur, B., Y. P. Kahya, E. Çağatay Güler and T. Engin, "Comparison of AR-based algorithms for respiratory sounds classification", *Computers in Biology and Medicine*, Vol. 24, No. 1, pp. 67 – 76, 1994, `http://www.sciencedirect.com/science/article/pii/0010482594900388`.